AIR FORCE INSTITUTE OF TECHNOLOGY

AIR UNIVERSITY
UNITED STATES AIR FORCE

SCHOOL OF ENGINEERING

WRIGHT-PATTERSON AIR FORCE BASE, OHIO

DISCLAIMER NOTICE

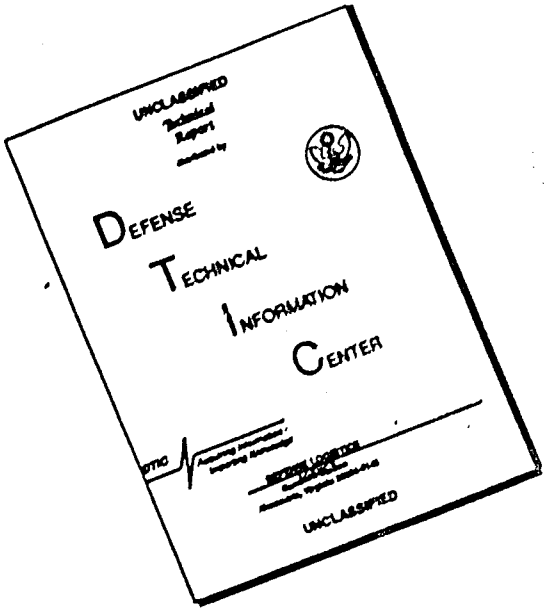

THIS DOCUMENT IS BEST QUALITY AVAILABLE. THE COPY FURNISHED TO DTIC CONTAINED A SIGNIFICANT NUMBER OF PAGES WHICH DO NOT REPRODUCE LEGIBLY.

UNCLASSIFIED
Security Classification

DOCUMENT CONTROL DATA - R & D

(Security classification of title, body of abstract and indexing annotation must be entered when the overall report is classified)

1. ORIGINATING ACTIVITY (Corporate author) Air Force Institute of Technology (AFIT-SE) Wright-Patterson AFB, Ohio, 45433	2a. REPORT SECURITY CLASSIFICATION Unclassified 2b. GROUP

3. REPORT TITLE

ANALYSIS OF PILOTED WEAPON DELIVERY: F-4E AERIAL GUNNERY

4. DESCRIPTIVE NOTES (Type of report and inclusive dates)

AFIT Thesis

5. AUTHOR(S) (First name, middle initial, last name)

Richard H. Hackford Jr.
Capt USAF

6. REPORT DATE	7a. TOTAL NO. OF PAGES	7b. NO. OF REFS
June 1972	86	23

8a. CONTRACT OR GRANT NO.	9a. ORIGINATOR'S REPORT NUMBER(S)
b. PROJECT NO.	GGC/EE/72-3
c.	9b. OTHER REPORT NO(S) (Any other numbers that may be assigned this report)
d.	

10. DISTRIBUTION STATEMENT

Approved for public release; distribution unlimited

Approved for public release; IAW AFR 190-17

Keith A. Williams, 1st Lt., USAF Acting Director of Information	12. SPONSORING MILITARY ACTIVITY Air Force Flight Dyanmics Laboratory Wright-Patterson AFB, Ohio

13. ABSTRACT

Research was conducted to determine the effect of F-4E aircraft dynamics upon pilot tracking capability in the aerial gunnery mission. An example firing situation was postulated and the characteristics of the resulting lead-pursuit trajectory were determined. Mathematical representations of the aircraft; the flight control system dynamics; the fire control system dynamics, the turbulence environment, and the pilot were used to predict tracking error. The fire control system was assumed to compute the correct aimpoint, and the projectile terminal miss distance due to pilot tracking error was computed using an iterative scheme. The results of this analysis were then compared with a baseline F-4C strafing case and found to be similar in trend but greater in magnitude.

DD FORM 1 NOV 68 1473

UNCLASSIFIED
Security Classification

14. KEY WORDS	LINK A		LINK B		LINK C	
	ROLE	WT	ROLE	WT	ROLE	WT
Analytic Pilot Modeling						
Aerial Gunnery						
Weapon Delivery Analysis						

ANALYSIS OF PILOTED WEAPON DELIVERY: F-4E AERIAL GUNNERY

THESIS

GGC/EE/72-3 Richard H. Hackford, Jr.
Capt. USAF

Approved for public release; distribution unlimited.

ANALYSIS OF PILOTED WEAPON DELIVERY:
F-4E AERIAL GUNNERY

THESIS

Presented to the Faculty of the School of Engineering

of the Air Force Institute of Technology

Air University

in Partial Fulfillment of the

Requirements for the Degree of

Master of Science

by

Richard H. Hackford, Jr., B.S.

Captain USAF

Graduate Guidance and Control

June 1972

id

DEDICATION

During 1966 I was privileged to fly the Republic F-105D Thunderchief with the 469th Tactical Fighter Squadron stationed at Korat Royal Thai Air Force Base, Thailand. For a majority of this tour I was assigned to "A" Flight of that squadron and flew most of my missions with the other five members of the flight. I wish to dedicate this work to two of my fellow pilots who were not as lucky as I:

to Major Dane Milliman who was killed when his aircraft exploded during takeoff, crashed, and burned,

and to Captain David J. Earll who failed to pull out of a dive bomb run one day while looking for SAM sites.

Preface

I wish to thank Major Robert R. Rankine, Jr., Assistant Professor of Electrical Engineering at the Air Force Institute of Technology, for his continued assistance and encouragement throughout this study. He managed to transform this degree requirement into the most valuable learning experience I have had at this school.

I also wish to thank Captain Robert Hovde and Lt. William Hartman for allowing me to use their matrix multiplication and integration computer programs, respectively.

Next, I wish to express my deep gratitude to Mrs. Virginia Blakelock, who made this final manuscript directly from my initial handwritten notes. The excellence of form displayed by this work is an eloquent testimony to her skill, patience, and dedication to perfection. I could not have completed this effort on time without her aid.

Finally, all mistakes of substance are my responsibility. With computations as long and complex as the ones in this thesis, human errors are bound to occur.

Richard H. Hackford, Jr.

Contents

	Page
DEDICATION	ii
Preface	iii
List of Figures	vi
List of Tables	viii
List of Symbols	ix
Abstract	xii
I. Introduction	1
II. The Aerial Gunnery Mission	5
Introduction	5
Aerial Gunnery Mission	5
Example Firing State	5
Aerial Gunnery System	9
General Discussion	9
Fire Control System	9
Sight Reticle	11
Pilot Control Tasks	13
Control Input	17
Performance Criterion	19
III. Prediction of Tracking Performance	20
Analytic Pilot Modeling	20
Lateral Input and Controlled Element	23
Roll Control	27
Lateral Tracking	38
Longitudinal Input and Controlled Element	45
Longitudinal Tracking	48
Homogeneous Pilot Model	54
Special Longitudinal Case	56
IV. Mathematical Model of the Aerial Gunnery Task	58
Introduction	58
Prediction Angle	58
Description	58
Lead	58
Curvature Correction	59
Jump Correction	61

Contents

	Page
Determination of the Nominal Trajectory	62
Introduction	62
Calculation of Prediction Angle	63
Correcting the Prediction Angle for Projectile Drag	64
Correcting the Prediction Angle for Angle of Attack	67
Computed Example Firing Situation	68
Calculation of Projectile Miss Distance	69
V. Conclusions and Recommendations	73
Introduction	73
Analysis of Results	73
Baseline Comparison	75
Recommendations for Further Study	76
Discussion of the Analysis Procedure	76
Bibliography	78
Appendix A: F-4E Aircraft Characteristics	80
Vita	86

List of Figures

Figure		Page
1	Tracking Line Reference System	7
2	Sight Reticle	12
3	The Geometry of Lateral Pipper Displacement	16
4	Quasi-Linear Model of Compensatory Tracking by a Pilot	22
5	A Model of the Effect of Vertical Gusts on the Lateral Dynamics of an Aircraft	24
6	A Model of the Effect of Side Gusts on the Lateral Dynamics of an Aircraft	25
7	Comparison of Lateral Disturbance Inputs (Roll Loop)	29
8	Controlled Element Characteristics (Roll Loop)	31
9	Roll Angle Control System	33
10	Roll Angle Perturbation vs Pilot Gain	35
11	Forward Transfer Function Characteristics (Roll Loop)	37
12	Comparison of Lateral Disturbance Inputs (Tracking Loop)	39
13	Lateral Tracking Control System	41
14	Model of the Effect of Vertical Gusts on the Longitudinal Dynamics of an Aircraft	47
15	Longitudinal Tracking System	50
16	System Crossover Frequency vs Pilot Gain	53
17	Lead Angle Geometry	59
18	Gravity Drop Geometry	60
19	Velocity Jump Geometry	62
20	Jump Angle Condition	63
21	Longitudinal Variance Interaction	70
22	Lateral Variance Interaction	70

List of Figures

Figure		Page
23	F-4E Elevon Control System	83
24	F-4E Rudder Control System	84
25	F-4E Aileron Control System	85

List of Tables

Table		Page
I	Firing State Parameters	8
II	Example Firing Situation Parameters	69

List of Symbols

A - K	general transfer functions
A	aileron; angle of muzzle deflection due to roll
A_β	drag coupling coefficient
B	body; effective angle of muzzle depression due to roll
C	coefficient; angle of sight deflection due to roll; gravity drop angle
D	effective angle of sight depression due to roll; range; drag
E	earth; elevon; expected value; elevation angle
F	final; foveal; force
I	lag; input; moment of inertia
J	jump angle
J_v	ballistic jump parameter
K	constant; sensitivity; coefficient
L	lift; characteristic length; x-axis moment coefficient; lead angle
M	y-axis moment coefficient; Mach number
N	numerator; z-axis moment coefficient
P	pilot; pitch; remnant parameter; projectile; pipper
Q	general transfer function
R	remnant; rudder; roll; general transfer function
S	wing area; scanned; scaling area
T	total; time; time constant; general transfer function; target
T_f	projectile time of flight
TLX	forward or along track axis of tracking line reference system
TLY	azimuth or cross track axis of tracking line reference system
TLZ	elevation axis of tracking line reference system

U	forward velocity
V	velocity; vertical
V_f	average projectile velocity
W	weight
Y	y-axis force coefficient; yaw
Z	z-axis force coefficient
a	aileron; acceleration; attacking aircraft
$\bar{a}_n$	normal acceleration
b	wing span
c	crossover; control; controlled element
$\bar{c}$	mean aerodynamic wing chord
d	deflection
e	error; elevation; effective
g	acceleration due to gravity; gust
h	altitude
i	initial; input; along-track unit vector
j	imaginary; cross-track unit vector
k	downward unit vector
m	muzzle, remnant; mass
n	nominal
o	equilibrium; trim; optimum
p	pilot; roll rate
q	dynamic pressure; pitch rate
r	range; noise signal; rudder; yaw rate
s	Laplacian operator; side; unit vector along tracking line
v	vertical; component of velocity perturbation in direction of right wing

w	downward component of velocity perturbation
x	forward or along-track axis
y	right-wing or cross-track axis
z	downward axis; unit vector along vertical
Δ	perturbation; difference; denominator
Ω	pitch attitude
Σ	sight depression angle
Φ	roll attitude; power spectrum density
Ψ	yaw attitude
α	angle of attack
β	angle of sideslip; line of sight angle
δ	control or surface deflection
ϵ	gun depression angle; error
η	mean; noise signal
θ	perturbation pitch attitude
λ	target aircraft flight path angle; vector prediction angle
μ	perturbation lateral tracking error
ξ	gun angle of attack
ρ	air density; target aircraft heading; target angle off
σ	standard deviation, rms intensity
σ^2	variance; mean square intensity
τ	time delay
ϕ	perturbation roll attitude
ψ	perturbation yaw attitude
ω	frequency
$(\dot{})$	rate of change of

Abstract

Research was conducted to determine the effect of F-4E aircraft dynamics upon pilot tracking capability in the aerial gunnery mission. An example firing situation was postulated and the characteristics of the resulting lead-pursuit trajectory were determined. Mathematical representations of the aircraft, the flight control system dynamics, the fire control system dynamics, the turbulence environment, and the pilot were used to predict tracking error. The fire control system was assumed to compute the correct aimpoint, and the projectile terminal miss distance due to pilot tracking error was computed using an iterative scheme. The results of this analysis were then compared with a baseline F-4C strafing case and found to be similar in trend but greater in magnitude.

ANALYSIS OF PILOTED WEAPON DELIVERY: F-4E AERIAL GUNNERY

I. Introduction

The principal objective in designing an aircraft should be the creation of a system which allows the pilot to accomplish the intended mission with maximum effectiveness. Until recently, however, this design goal could not be achieved directly as no analytical theory existed which related aircraft design parameters to mission success criteria.

The primary obstacle to developing such a system theory of aircraft design was the lack of knowledge of the performance characteristics of the pilot. In many situations, including the one described in this report, the pilot acts as a feedback controller using information about the current aircraft state to generate commands to complete his assigned mission. Thus, the major consequence of this inability to mathematically model the pilot was that the designer could analytically define only a portion of the forward transfer function consisting of the aircraft, the flight control system, the fire control system, and any other subsystems included in the signal path between the pilot's input and the aircraft controlled variables. This state of affairs produced two major effects.

First, aircraft design goals were stated in terms of open loop dynamic parameters (Ref 4). Empirical data showed that if an aircraft exhibited certain response characteristics, the pilot would be able to accomplish his mission. No claim was made that the properly designed aircraft would allow the pilot to do this in the most efficient manner.

Second, aircraft subsystems were treated as separate entities rather than as components of a total system. Since the contribution of

each functional unit to the dynamic characteristics of the entire system and the interaction of these units could not be determined, the design approach was to optimize each item as a separate entity regardless of the effect upon the total system. Thus, the emphasis of design improvement tended to be concentrated at the subsystem level as evidenced by the continued reduction of weapon anomalies, development of more accurate sensors, improvement of computation schemes, reduction of component tolerances, and a host of other innovations. It was assumed without question that these subsystem improvements would create a more efficient system (Ref 17:1).

This situation began to change in the 1960s when McRuer, Levison, and many others, began a series of continuing investigations into the nature of pilot control policies (Refs 9, 10, and 12). They were able to develop describing functions which had the same average output characteristics and produced the same performance levels that a pilot did when confronted with the identical control task. These pilot describing functions provided the designer with a powerful analytic tool; they could be combined with the aircraft system descriptions to form a closed loop model of the entire process. Thus, the designer now had the capability to relate aircraft system parameters to mission performance.

In 1967, McRuer and Jex developed an analytical technique which represents a systems approach to aircraft design (Ref 13:9-28). Major Robert R. Rankine, Jr., an Assistant Professor of Electrical Engineering at the Air Force Institute of Technology, identified the elements of this theory for weapon delivery and analyzed the performance of the F-4C aircraft in the strafing role (Ref 17). The basis for the theory is the prediction of system performance using an analytical model of the pilot;

the method, which is valid for a wide variety of aircraft missions, proceeds in the following manner.

First, a mission is selected and a performance criterion is formulated to measure the effectiveness of the pilot-aircraft system in accomplishing this mission. Next, the tasks that the pilot must perform in order to complete the mission are determined and then all elements of the aircraft and its associated subsystems which the pilot will use to accomplish this mission are identified and described mathematically. Models are developed relating the aircraft controlled variables to both pilot and disturbance inputs; then mathematical relationships are generated which associate a particular value of the performance measure with each aircraft state defined by the controlled variables. The end result is an analytical model which relates the form and values of various parameters of the pilot-aircraft system to the measure of mission effectiveness (Ref 17).

In this study, the systems analysis method just described is applied to the aerial gunnery mission. In order to completely define the situation, to fully illustrate the procedure, and to provide numerical results, an example firing state is postulated and the F-4E aircraft is selected as the system to be analyzed. To successfully complete this mission, the pilot is required to hold an aim point, the pipper, on the target aircraft while firing the cannon; this task is defined to be target tracking. The primary purpose of this thesis is to show the effects that flight control system and fire control system dynamics have upon pilot tracking performance.

The analysis begins in Chapter II with a discussion of the aerial gunnery mission and the definition of a nominal firing state to serve as an illustrative example of this mission. Next, the pilot control tasks are determined and the subsystems which are used by the pilot to accomplish

the mission are described. Finally, an appropriate performance measure is selected. In Chapter III, two mathematical models are developed which relate pilot tracking performance to disturbance inputs. This is accomplished by perturbing the attacking aircraft from its nominal firing state with turbulence inputs and then measuring the pilot's ability to return the aircraft to the nominal state. A final model is formulated in Chapter IV to assign a specific value to the performance measure for each level of pilot tracking performance. In Chapter V the conclusions which can be drawn from this analysis are presented.

The systems theory of aircraft design employed in this thesis is a powerful method which has unique capabilities and great versatility. It can be used to predict the performance of an aircraft in all weapon delivery roles and provides a means for comparing different aircraft employed in the same mission. It also allows the analytic evaluation of proposed design improvements. Since the factors which degrade performance are analytically identified and ranked in order of relative importance by this procedure, deficiencies may be corrected in the logical order of their contribution to the performance measure. This is a powerful tool for the manager as it enables him to make more effective use of his limited resources. Applied on a large scale, the method could be used to identify basic airframe characteristics and base line subsystems in the flight control system and the fire control system which would be required to achieve a given acceptable level of mission performance. Finally, if probability of mission success is used as a performance criterion, the military strategist could employ this procedure to determine the force levels required to achieve given strategic and tactical objectives and to compare his resources to those of the opponent to determine the probability of success in a given military venture (Refs 18 and 19).

II. The Aerial Gunnery Mission

Introduction

In this chapter the aerial gunnery mission is discussed and an example firing situation is postulated. The closed-loop control system responsible for accomplishing the mission is described and the functions of various components of this system are examined. Finally, an appropriate performance criterion is selected.

Aerial Gunnery Mission

The objective of the aerial gunnery mission is to score projectile hits upon the target aircraft; the pilot achieves this goal by flying his aircraft to a required attitude and holding this attitude while firing the cannon (Ref 8:1). The fire control system determines the correct aircraft attitude and supplies this information to the pilot via an aiming dot. As the attacking aircraft moves in space, the fire control system continuously computes the firing states which comprise the lead-pursuit trajectory. The pilot remains on this trajectory by superimposing the aiming dot on the target aircraft; a projectile hit is guaranteed if the pilot fires the cannon while on this nominal trajectory. There are literally an infinite number of lead-pursuit trajectories based upon the target and the attacking aircraft states; therefore, an example firing situation will be stated and used to highlight certain aspects of the aerial gunnery mission and to illustrate the analytical techniques applied in this study.

Example Firing State

The description of the example firing state begins with the definition

of two terms. The weapon line is defined to be the extension of the cannon bore and is colinear with the muzzle velocity vector of the projectile; the tracking line is the line from the pilot's eye which passes through the aiming dot. The weapon line and the tracking line are initially considered to be colinear; then, the target aircraft is located at a range of 2000 feet along the combined weapon and tracking lines. In the absence of aircraft motion and field effects (gravity, projectile drag), firing the aircraft cannon from this position would result in a hit on the target.

Next, the two aircraft are set in motion. Initially, the attacking aircraft's velocity is 0.9 Mach and is assumed to be along the combined weapon and tracking lines. For computational purposes, it is necessary to reference the target aircraft's velocity vector to the tracking line. Hence, a tracking line reference system is defined and illustrated in Fig. 1, where

TLX is measured along the tracking line,

TLY is measured in the plane perpendicular to the tracking line and parallel to the local horizontal,

TLZ is measured in the plane perpendicular to the tracking line and is also perpendicular to the TLY axis,

ρ is the target aircraft heading measured positively in a clockwise sense about the TLZ axis, and

λ is the target aircraft flight path angle measured positively in a counterclockwise sense about the displaced TLY axis.

In this example, the target aircraft has a velocity of .8 Mach, a heading of 0°, and a flight path angle of 0°; it is further assumed that the target

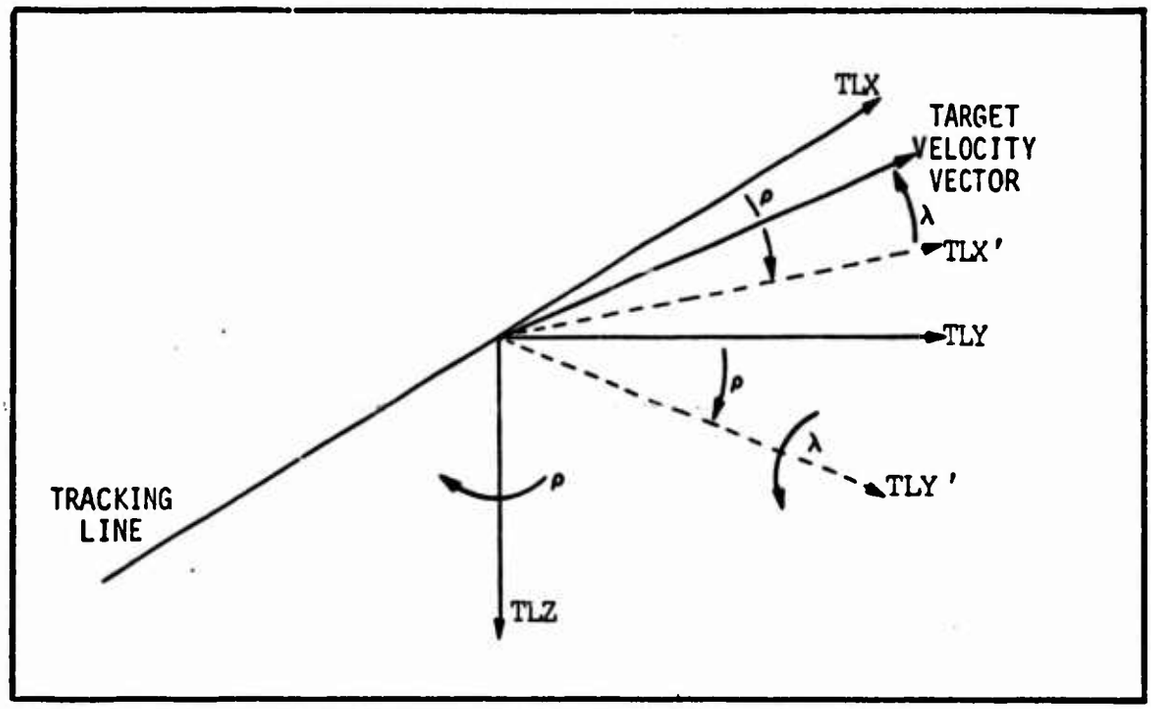

Fig. 1. Tracking Line Reference System

is in unaccelerated flight and will remain in that condition during the projectile time-of-flight.

When field effects and aircraft motion are included in the example firing situation, it becomes necessary to create the proper angle between the weapon line and the tracking line while holding the tracking line on the target aircraft to insure projectile hits. This angle is called the prediction angle and is determined by the fire control system of the attacking aircraft. The calculation of the prediction angle for this example firing situation is covered in detail in Chapter IV; additionally, some of the functional aspects of the computation of this angle by the fire control system are discussed in the next section.

To complete the specification of the example firing state, both aircraft are assumed to be flying at an altitude of 15,000 feet mean sea level and the attacking aircraft, an F-4E, is operating at a weight of 46,600 pounds.

This case represents one of the simplest firing situations that could occur for the attacking aircraft. Both aircraft are travelling in the same direction, the F-4E is within firing range, and is overtaking the target aircraft directly from the rear. The parameters of the firing state were dictated by the limits of validity of the pilot model and by the desire to reduce computational errors within the fire control system to zero. In spite of the seeming simplicity of the situation, however, the aircraft dynamics do exert a powerful influence upon the pilot tracking performance as will be shown and, since the objective of this work is to demonstrate the relationship between these two items, the firing situation is sufficiently rigorous for the purposes of this analysis.

A summary of the parameters of the example firing state is presented in Table I.

TABLE I
Firing State Parameters

Target range	2000 ft
Target aircraft:	
Heading	0 deg
Flight path angle	0 deg
Mach number	0.8
Velocity	845.9 ft/sec
Attacking aircraft:	
Mach number	0.9
Velocity	951.6 ft/sec
Altitude	15,000 ft
Weight	46,159 lb

Aerial Gunnery System

General Discussion. The aerial gunnery system is defined to encompass the pilot, the aircraft and its associated dynamics, the flight control system including all stability augmentation, the fire control system including all appropriate measurements, computations, and displays, and the aircraft mounted cannon, a 20 mm Gatling gun.

For purposes of this analysis, it is assumed that the attacking aircraft has achieved stabilized tracking on the nominal lead-pursuit trajectory. Thus, the radar is locked on to the target, the fire control system is computing and displaying the correct aimpoint, and the pilot has placed the aimpoint on the target aircraft. The net effect is that there are no transients within the aerial gunnery system.

Several salient features of the aerial gunnery system will now be discussed; the intent is to provide insight into the operation of the system, derive the control laws which must be implemented if the mission is to succeed, and to describe the limitations of the system.

Fire Control System. The F-4E Fire Control System consists of the sight reticle, the lead-computing amplifier, and the lead-computing gyroscope; the purpose of these components is to solve Eq (1) for the prediction angle and display this information to the pilot (Ref 7:2-1).

$$\bar{\lambda} = T_f \dot{\bar{\beta}} - J_v \frac{V_a}{V_f} \bar{\alpha} + \frac{T_f}{2V_f} (\bar{s} \times \bar{a}_n) + \frac{DT_f}{2V_f} \ddot{\bar{\beta}} - \frac{(1 - A_\beta) g T_f}{2V_f} (\bar{s} \times \bar{z}) \qquad (1)$$

lead for target motion across the line of sight	jump correction	gravity drop and attacker acceleration	line of sight acceleration	cross effect of gravity drop and projectile drag

where

$\bar{\lambda}$ = vector prediction angle,

T_f = projectile time of flight,

$\dot{\bar{\beta}}$ = angular velocity of the line-of-sight,

J_v = ballistic jump parameter,

V_a = attacker velocity,

V_p = average projectile velocity relative to the attacking aircraft,

$\bar{\alpha}$ = gun angle of attack,

$\bar{s}$ = unit vector along tracking line,

$\bar{a}_n$ = normal acceleration,

D = range,

A_β = drag coupling coefficient, and

$\bar{z}$ = unit vector along vertical.

Unfortunately, the system can compute only the first three terms of Eq (1) due to measurement problems (Ref 7:2-2). Therefore, if there are to be no computational errors in the problem, the example firing situation must be constructed in such a manner that the final two terms are truly zero; it is for this reason that both the target aircraft and the attacking aircraft were constrained to unaccelerated flight. Unfortunately, this requirement also reduces the first term, lead for target motion, to zero; hence, the final computations include only gravity drop, jump angle, and projectile drag effects. For the example firing situation, then, Eq (1) reduces to Eq (123), Eq (128), and Eq (130) of Chapter IV and the prediction angle calculated by the fire control system is the same as the true prediction angle.

The lead pursuit tracking task is an inherently unstable situation; to remedy this fact, a lag is incorporated in the fire control system.

This lag is called the "stability number" and is .25 for the F-4E (Ref 8:15). Thus, there is a delay between the calculation of a given prediction angle and the display of this information to the pilot. In certain dynamic situations, then, the sight reticle is indicating an incorrect aiming point. Since sight instability is most pronounced during the initiation of target tracking and under high attacking aircraft acceleration conditions and, since the example firing situation is an extremely benign case, the sight stability number will be considered to be zero in this study and it will be assumed that the aim dot is indicating the correct firing information at every instant of time.

This completes the discussion of the unique features and limitations of the fire control system. There are several other error generating factors in this situation; they all have a relatively minor effect on the problem solution, are briefly discussed in Chapter IV, and are neglected for the purposes of this analysis. Fire control system computational errors are ignored for the remainder of this study; if the pilot fires the cannon with the aim dot on the target, it is assumed that the projectile will hit the target aircraft.

Sight Reticle. The information necessary to create the required prediction angle is presented to the pilot in the form of a sight reticle; this reticle is a visual pattern displayed on the optical sight unit. The optical sight unit is mounted on top of the center of the instrument panel and is the only instrument used by the pilot to accomplish the aerial gunnery mission. The sight reticle is illustrated in Fig. 2 (Ref 20:1-121).

The sight reticle is initially aligned with the weapon line as discussed in the example firing situation. After a radar lock-on has been

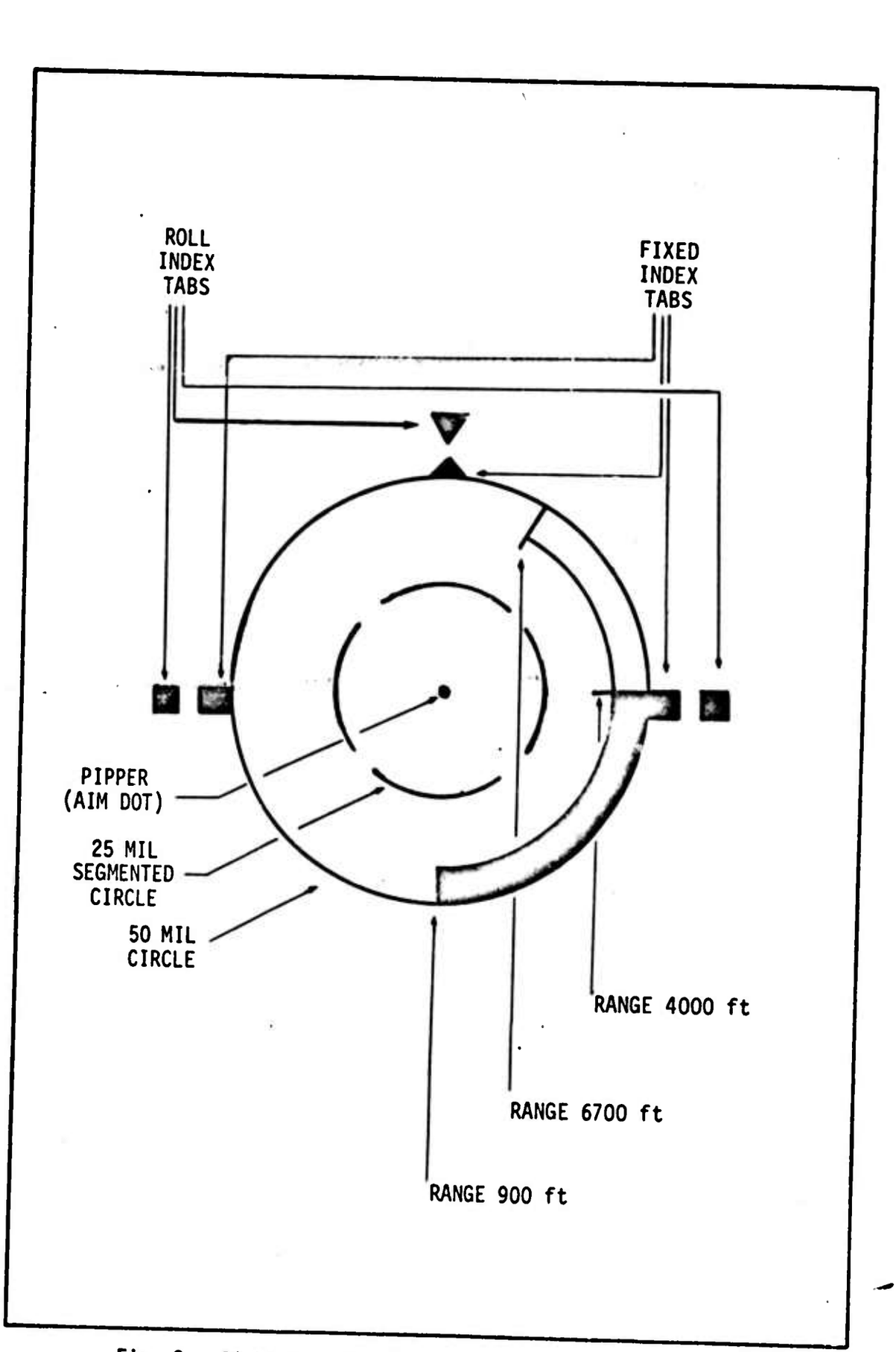

Fig. 2. Sight Reticle (Adapted from Ref 20:1-121)

achieved and the prediction angle has been computed, the sight reticle moves downward on the optical sight unit through the prediction angle; the pilot then flies the pipper (aim dot) back up to the target aircraft. This action raises the weapon line above the target in the target's direction of travel by the required prediction angle; thus, the firing attitude required to achieve a hit on the target has been established.

The fire control system will generate prediction angles for ranges varying from 900 feet to 4000 feet. The pilot may fire then anytime the range bar indicates a range between these two extremes (Ref 20:124). The range bar indicates a range of 6700 feet when fully expanded, 4000 feet at the state shown in Fig. 2, and 900 feet when fully contracted at the bottom of the reticle. The bar operates like a thermometer, reducing the amount of red field displayed as range decreases. The gun is optimized for a range of 2250 feet and, without radar range information, the prediction angle is calculated on the basis of a 1500-foot range. The pilot is therefore more likely to fire in this interval of ranges and, as a result, a target range of 2000 feet is used in the example firing situation. There is one other set of competing considerations in selecting a firing range. Changes in the target acceleration during the projectile time of flight will result in a terminal error. This error can be minimized by firing at shorter ranges; however, the attacking aircraft runs the risk of colliding with the target or hitting target debris. All of these factors, then, generally result in firing ranges from 1500 feet to 2500 feet and, therefore, the firing range in the example firing situation is certainly realistic.

Pilot Control Tasks. As the attacking aircraft moves along the nominal lead-pursuit trajectory, it is disturbed from this path by atmospheric

turbulence; the pilot views this perturbation from the nominal state as both lateral and longitudinal displacement of the pipper from the target aircraft. In order to accomplish the aerial gunnery mission, the pilot must return the pipper to the target; to do this, he must perform three distinct control tasks.

The pilot's first concern is to maintain the nominal trajectory to insure future firing opportunities and he achieves this by properly controlling the roll angle of the attacking aircraft. Referring to Fig. 1, page 7, the TLY-TLZ plane is called the maneuver plane. The attacking aircraft must move in the same direction in this plane as the target aircraft does to insure continued tracking. The pilot accomplishes this goal by predicting the future position of the target from its present attitude, velocity and acceleration and then flying the pipper to this predicted position. This estimate is easy to make in the example firing situation; the target aircraft is located directly ahead of the attacker, has no velocity in the maneuver plane, and, as it can only accelerate in the maneuver plane along its lift line, its vertical tail points in the direction of its next most probable position. Therefore, the pilot will attempt to maintain the same roll attitude as the target aircraft; this will enable him to maintain a stable lead-pursuit trajectory by using his acceleration capability to move with the target in the maneuver plane.

The example firing situation contains one subtle element which is crucial to the success of this analysis. For the analytic pilot modelling technique to be valid, the pilot must have an explicit error signal upon which to operate (Ref 12:240). Here, the upper index of the sight reticle and the vertical tail of the target aircraft provide an explicit measure of bank angle error. As the target aircraft achieves an angle off, however,

it begins to have a velocity component in the maneuver plane, and bank angle no longer provides an adequate cue to the future position of the target. The pilot then relies on his experience to determine the probable future position of the target from the complex mixture of target attitude, velocity, and acceleration. Since the pilot is no longer operating on an explicit error signal, one of the constraints of the analytical pilot modelling technique is no longer satisfied and there is no assurance that the model can be used. Thus, the parameters of the example firing situation were selected to specifically satisfy the requirements of the analytical pilot model.

Having achieved a stable nominal trajectory, the pilot next acts to eliminate the lateral displacement of the pipper. The lateral error in pipper placement perceived by the pilot is due to yaw perturbation (ψ) and a component of roll (ϕ) caused by the depression of the tracking line below the velocity vector, the axis of roll of the aircraft; the geometry of the situation is shown in stability axis in Fig. 3. From Fig. 3 and the relations for spherical triangles,

$$\frac{\sin \phi}{\sin C} = \frac{\sin(\pi/2)}{\sin(\Sigma - \alpha_0)} = \frac{\sin(\pi/2 - \phi)}{\sin D} \tag{2}$$

where Σ is the sight depression angle in radians, and α_0 is the aircraft angle of attack on the nominal trajectory. Since $\sin(\pi/2) = 1$ and $\sin(\pi/2 - \phi) = \cos \phi$, this gives the relations:

$$\sin C = \sin \phi \sin(\Sigma - \alpha_0) \tag{3}$$

$$\sin D = \cos \phi \sin(\Sigma - \alpha_0) \tag{4}$$

When $\Sigma > \alpha_0$, a positive roll perturbation causes the pipper to move to the left of the target while a positive yaw perturbation always causes the pipper to move to the right of the target. Assuming the longitudinal

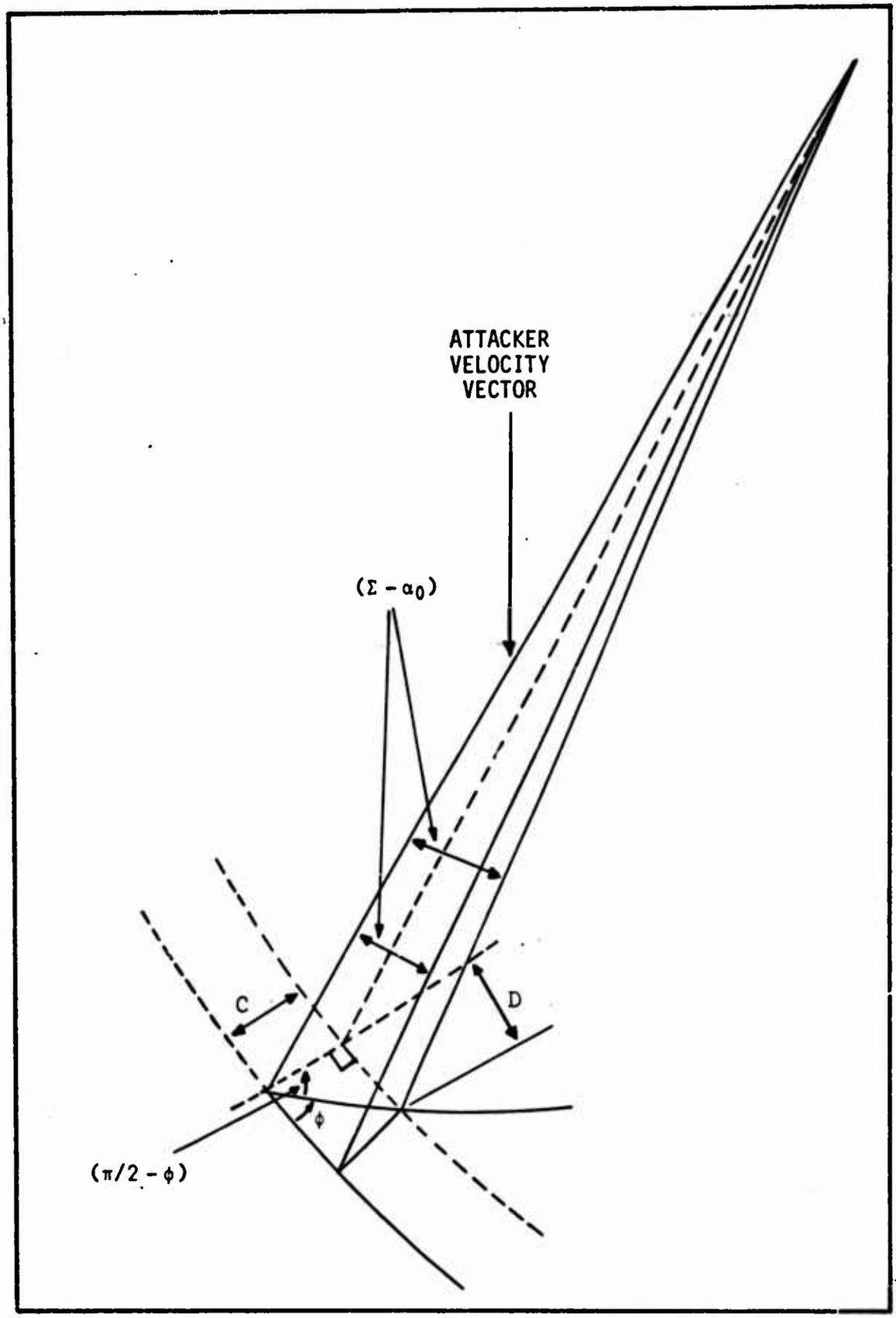

Fig. 3. The Geometry of Lateral Pipper Displacement (Adapted from Ref 17:25)

variables to be at their nominal values, the lateral tracking error observed by the pilot can be expressed as

$$\mu = \psi - C \tag{5}$$

where from Eq (3),

$$C = \sin^{-1}[\sin \phi \sin(\Sigma - \alpha_0)] \tag{6}$$

Consistent with the small perturbation analysis being accomplished in this study, Eq (5) may be simplified to

$$\mu = \psi - (\Sigma - \alpha_0)\phi \tag{7}$$

Therefore, the lateral tracking task consists of controlling a linear combination of perturbation yaw and roll (Ref 17:22-24).

Finally, the pilot must eliminate the longitudinal displacement of the pipper from the target aircraft. When the attacking aircraft is disturbed from the nominal trajectory, a pitch perturbation angle (θ) is created. The lead computing gyroscope senses the rate of this angle and commands a new pipper position on the optical sight unit. Thus, the pilot observes and must control a combination of perturbation pitch angle (θ) and perturbation pipper position (θ_p).

Control Input. The final function in the sequential description of the aerial gunnery system is the generation of the appropriate controls to place the pipper on the target. In the longitudinal tracking case, a pitch input at the stick is the only control that is available to the pilot. In the roll angle and lateral tracking tasks, however, the pilot has two control inputs available; the pilot may command aileron, rudder, or a combination of these two controls.

The pilot can adopt three distinctly different strategies in the case of lateral-directional control inputs. He may use aileron or rudder alone

or he may use one input as a primary control and the other input as a secondary control. An example of this policy is the introduction of aileron to create a given bank angle and turn rate and then, in a secondary role, the introduction of rudder to prevent slipping or skidding. Here the pilot uses aileron to accomplish his task and rudder to reduce undesirable consequences of the primary control action. Finally, a pilot may use both rudder and aileron in a primary control sense. An excellent example of this situation is the simultaneous application of rudder and aileron to create a sideslip for a crosswind landing. Once the controls have taken effect, the pilot will alter one or both inputs to achieve his objective. Here, one is unable to describe either input as a secondary control. A well-trained pilot will select the optimum control or mix of controls to accomplish his mission; further, the pilot with experience in a particular aircraft has learned exactly the magnitude and phasing of control inputs required to successfully complete his mission.

In this analysis, an aileron command is the control input applied to accomplish the roll angle and lateral tracking tasks. The author's experience in tactical aircraft similar to the F-4E supports this assumption for the low angle of attack situation studied here. Since the author has no flying experience in the F-4E and therefore is unfamiliar with the pilot control strategies peculiar to that aircraft, no secondary rudder commands will be used in the example firing situation to counter the effects of proverse yaw. However, at high angles of attack and at high normal acceleration levels, the rudder becomes an extremely effective control for maneuvering and tracking. Therefore, in each firing situation, some thought must be given to pilot control policies; it cannot be automatically assumed that the pilot will only use aileron commands to accomplish the aerial gunnery

missions. The intent of this discussion, then, is to present an insight into the variety of control options open to the pilot in order that the reader may more fully understand the complexities of this particular analysis.

Performance Criterion

A performance criterion must be selected to measure the pilot's effectiveness in accomplishing the aerial gunnery mission. The magnitude of the perturbations of the controlled variables, the projectile terminal miss distance, and probability of kill are all meaningful expressions of the degree of task completion.

In this study, the magnitude of the perturbations of the controlled variables is selected as the performance criterion; the form in which these magnitudes are expressed, root mean square intensity, is explained in Chapter III. This criterion was selected as it provides a non-dimensional measure which can easily be compared to similar quantities in other flight conditions or missions. Miss distance, on the other hand, is meaningful only if target range is constant; one key variable in the aerial gunnery task is the target range and, consequently, miss distance constrains the analysis if it is used as a performance measure. Probability of kill places emphasis upon probability of mission accomplishment and therefore is very useful to the planner. However, it does not exhibit the source or magnitude of the individual errors and, thus, is not a useful tool for the engineer.

III. Prediction of Tracking Performance

The purpose of this chapter is to describe in detail the development of two mathematical models relating gust inputs to changes in the controlled variables of the attacking aircraft. The great significance of these equations is that they will permit the quantitative evaluation of perturbations in the tracking variables caused by a given turbulence input. Thus, the models will allow prediction of pilot tracking performance.

The critical element in the formulation of these relationships is the representation of the pilot as a linear element in a complex control system. Consequently, prior to deriving the desired transfer functions, the mathematical modeling of the pilot will be discussed.

Analytic Pilot Modeling

The pilot is a complex, non-linear, time varying, controller who defies complete mathematical description; however, in certain limited, well defined situations, a pilot's control policy is so consistent that it can be represented by a linear mathematical model. The model is not constrained to correspond in structure or methodology to the pilot but must exhibit, on the average, the same output characteristics for a given input and achieve the same measure of performance as a pilot would when confronted with the identical task.

One situation for which a well-documented and widely used pilot model exists is the compensatory tracking task. In this situation, the pilot observes the difference between a stationary random input and the output of a linear time-invariant process and uses the perceived error to generate a manual control input to the process (Ref 17:68-71).

Examination of the firing situation postulated in the previous chapter reveals that it exhibits all the characteristics of the compensatory tracking task. First, the pilot is controlling an aircraft and its associated dynamics which can be accurately represented as a linear, time-invariant system. Next, this plant is disturbed from its nominal trajectory by a stationary random input in the form of atmospheric turbulence. The pilot views this perturbation from the nominal state as a displacement of the pipper from the target aircraft and he generates a control input in the form of a stick or rudder movement to again superimpose the pipper on the target. Thus all the requirements of the compensatory tracking task have been satisfied by the example firing situation and it is valid, for purposes of analysis, to represent the pilot as a linear element in the control system.

The model of the compensatory tracking task is illustrated in Fig. 4. The pilot is represented by a linear element and a remnant, the latter accounting for that part of the pilot's output which is not linearly correlated with the input. The linear element of the model must account for the adaption of the pilot and consists of two distinct parts: (1) a generalized describing function form representing the pilot's capability to compensate, and (2) a set of rules for adjustment of the parameters of the describing function for the input and plant characteristics. The model permits prediction of pilot performance in terms of root mean square error (σ_e) when the bandwidth and root mean square amplitude of the input (σ_i) and the aircraft dynamics are known (Ref 17:68-69).

A simple describing function form that can be used to represent the pilot in the compensatory tracking task is (Ref 12:234)

$$Y_p = K_p\left(\frac{1 + j\omega T_L}{1 + j\omega T_I}\right)e^{-j\omega\tau_e} \qquad (8)$$

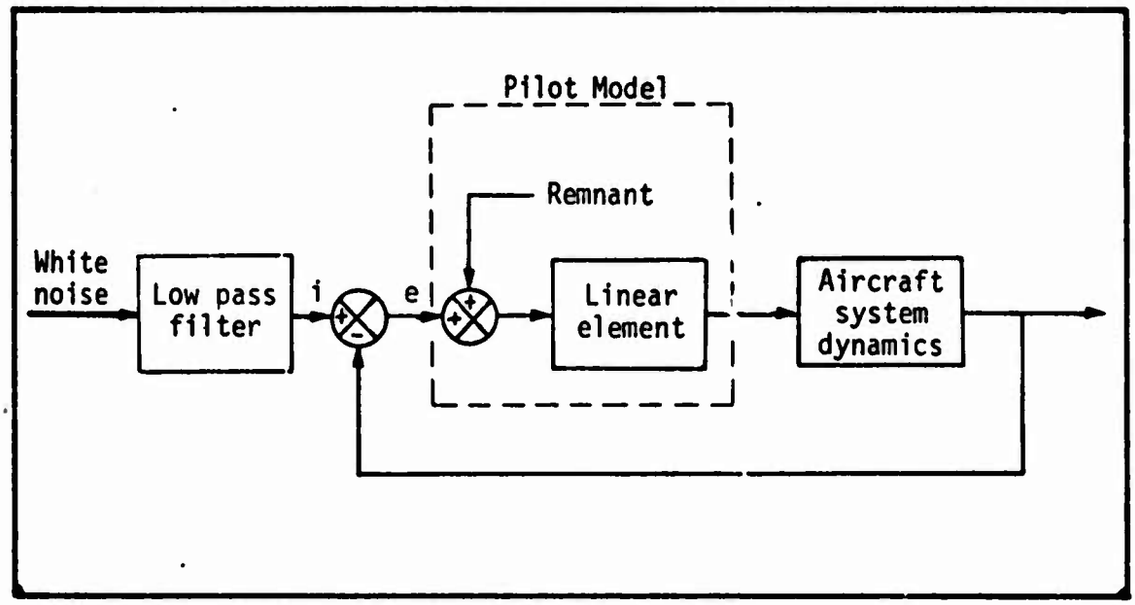

Fig. 4. Quasi-Linear Model of Compensatory Tracking by a Pilot (Adapted from Ref 12:240)

where

K_p = pilot static gain,

T_L = lead time constant,

T_I = lag time constant, and

τ_e = effective time delay including transport delays and high frequency neuromuscular lags.

The rules for adjusting the parameters of Eq (8) may be summarized as an attempt to achieve an open-loop transfer function near the crossover frequency of the form

$$Y_p Y_c = \frac{\omega_c}{j\omega} e^{-j\omega\tau_e} \tag{9}$$

where

Y_p = pilot describing function from Eq (8),

Y_c = transfer function of the controlled element,

ω_c = crossover frequency (loop gain), and

τ_e = effective time delay.

The transfer function of the controlled element Y_c must include the dynamics of the aircraft, the flight control system, the fire control system, and the appropriate displays. A comprehensive summary of the rules which establish the parameters of Eq (8) for both single axis and multi-axis compensatory tracking can be found in the paper by McRuer (Ref 12:231-248).

In the example firing situation, the pilot must perform three compensatory tracking tasks. In each case, an analytic pilot model of the form given in Eq (8) is employed and the adaption rules are discussed in greater detail and applied to determine the parameters of the model for that particular task.

Lateral Input and Controlled Element

In the example firing situation, the pilot has established himself on a nominal lead-pursuit trajectory and is presented with a series of firing opportunities which, if executed, would result in projectile hits upon the target aircraft. However, as he moves along this nominal trajectory, his aircraft is subject to two lateral disturbance inputs, a vertical turbulence spectrum which induces a roll rate and a horizontal turbulence spectrum which produces both a sideslip and a yaw rate. These gust inputs cause the aircraft to be perturbed off the nominal trajectory and the pilot observes this perturbation as a lateral displacement of the pipper from the target.

The roll rate disturbance produced by the continuous random vertical turbulence spectrum can be mathematically represented by a low-pass filtered white noise source. The filter dynamics can be represented as shown in Fig. 5, where

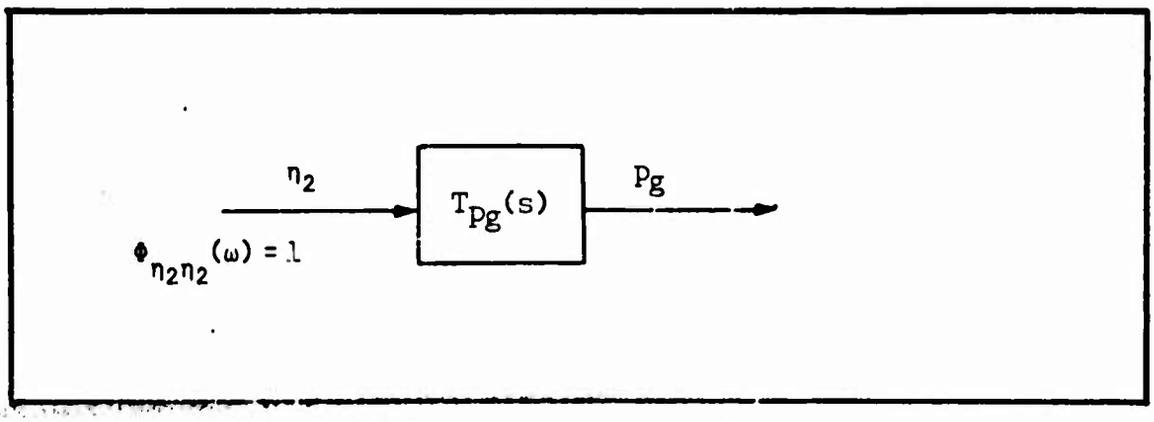

Fig. 5. A Model of the Effect of Vertical Gusts on the Lateral Dynamics of an Aircraft

$$T_{p_g}(s) = \sqrt{(1/L_w U_0)}\left(\frac{\sqrt{[.8(\pi L_w/4b)^{1/3}]}}{1 + 4bs/\pi U_0}\right)\sigma_w \tag{10}$$

η_2 = white noise signal, and

σ_w = rms intensity of the vertical gust in ft/sec

for the example firing situation:

L_w = 1750 ft = scale factor,

b = 38.41 ft = aircraft wing span, and

U_0 = 951.63 ft/sec = aircraft speed.

Hence,

$$\frac{p_g}{\eta_2} = \frac{(.0245)\sigma_w}{(s + 19.46)} \tag{11}$$

Similarly, the sideslip and yaw rate disturbances created by the continuous random horizontal turbulence spectrum can be represented by a low-pass-filtered white noise source which is uncorrelated with the noise source producing the rolling perturbation. The filter dynamics can be modelled as shown in Fig. 6, where (Ref 4:459)

$$T_{v_g}(s) = \sigma_v \sqrt{(L_v/\pi U_0)}\left(\frac{1 + \sqrt{(3)}L_v s/U_0}{(1 + L_v s/U_0)^2}\right) \tag{12}$$

η_1 = a white noise signal,

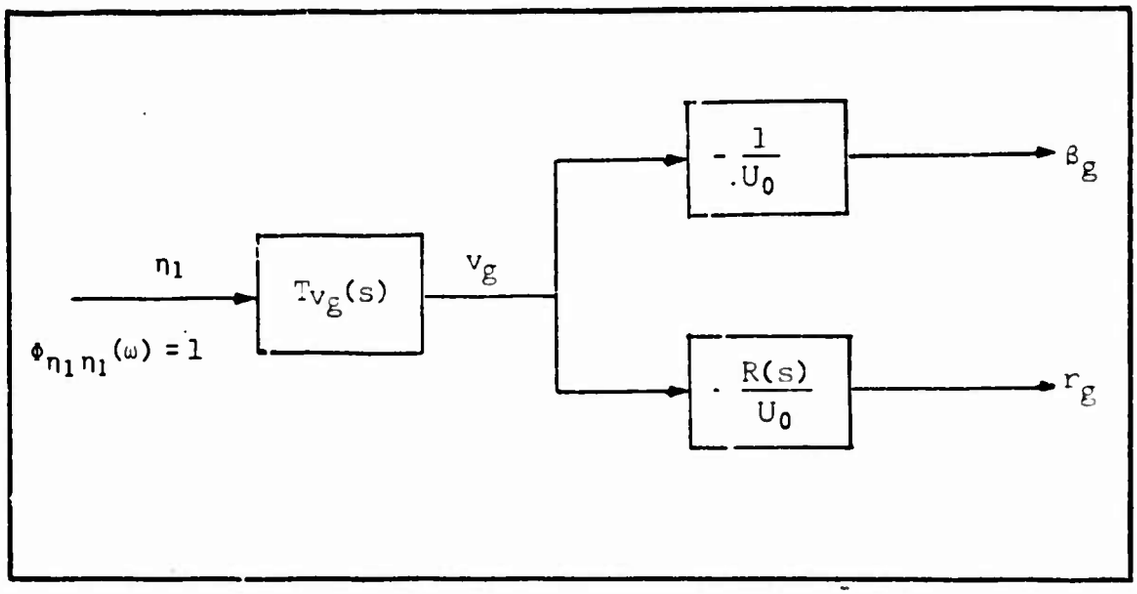

Fig. 6. A Model of the Effect of Side Gusts on the Lateral Dynamics of an Aircraft

σ_v = rms intensity of the side gust in ft/sec,

$$L_v = 145h^{1/3} \tag{13}$$

and

$$-\frac{R(s)}{U_0} = \frac{-(1/U_0)s}{1 + (3b/\pi U_0)s} \tag{14}$$

for the example firing situation:

h = 15,000 ft = aircraft altitude, and

L_v = 3576.01 ft = a scale factor.

Hence,

$$\frac{\beta_g}{n_1} = \frac{-.000530(s + .15)\sigma_v}{(s + .27)^2} \tag{15}$$

and

$$\frac{r_g}{n_1} = \frac{-(.0137)(s^2 + .15s)\sigma_v}{(s + 25.94)(s + .27)^2} \tag{16}$$

The lateral-directional equations of motion of the aircraft represent a portion of the controlled element dynamics as well as additional filtering

for the two gust inputs. For the gust inputs, as well as rudder and aileron inputs, the lateral directional equations are (Ref 1:112)

$$\begin{bmatrix} s-L_p & -L_r & -L_\beta \\ -N_p & s-N_r & -N_\beta \\ -sY_p-Y_\phi & -sY_r-Y_\psi & s^2-sY_\beta \end{bmatrix} \begin{bmatrix} p \\ r \\ \beta \end{bmatrix} = \begin{bmatrix} L_{\delta_r} & L_{\delta_a} & L_p & L_r & L_\beta \\ N_{\delta_r} & N_{\delta_a} & N_p & N_r & N_\beta \\ sY_{\delta_r} & sY_{\delta_a} & sY_p & sY_r & sY_\beta \end{bmatrix} \begin{bmatrix} \delta_{PR} \\ \delta_{PA} \\ p_g \\ r_g \\ \beta_g \end{bmatrix} \quad (17)$$

The aircraft dynamics are altered by the stability augmentation systems incorporated in the roll and yaw control channels. Hence they must be included in the above set of matrix equations.

The roll-axis control system can be depicted as (Ref 17:156-157)

$$\delta_a(s) = A(s)[\delta_{PA}(s) - B(s)p(s)] \quad (18)$$

where

$\delta_a(s)$ = aileron deflection,

$A(s)$ = power cylinder dynamics,

$\delta_{PA}(s)$ = lateral control stick deflection, and

$B(s)$ = roll rate feedback dynamics.

Similarly, the yaw axis control system can be represented as

$$\delta_r(s) = C(s)[\delta_{PR}(s) + D(s)r(s) + E(s)\beta(s)] \quad (19)$$

where

$\delta_r(s)$ = rudder deflection (positive left),

$C(s)$ = power cylinder dynamics and rudder flexibility,

$\delta_{PR}(s)$ = rudder pedal deflection (positive left forward),

$D(s)$ = yaw-rate feedback dynamics, and

$E(s)$ = sideslip feedback dynamics.

Substituting Eqs (18) and (19) into Eq (17) gives the following matrix equation relating the aircraft dynamic response to pilot and turbulence inputs:

$$\begin{bmatrix} s-L_p+ABL_{\delta_a} & -L_r-CDL_{\delta_r} & -L_\beta-CEL_{\delta_r} \\ -N_p+ABN_{\delta_a} & s-N_r-CDN_{\delta_r} & -N_\beta-CEN_{\delta_r} \\ -sY_p-Y_\phi+ABY_{\delta_a}s & -sY_r-Y_\psi-CDY_{\delta_r}s & s^2-sY_\beta-CEY_{\delta_r}s \end{bmatrix} \begin{bmatrix} p \\ r \\ \beta \end{bmatrix}$$

$$= \begin{bmatrix} CL_{\delta_r} & AL_{\delta_a} & L_p & L_r & L_\beta \\ CN_{\delta_r} & AN_{\delta_a} & N_p & N_r & N_\beta \\ CY_{\delta_r}s & AY_{\delta_a}s & sY_p & sY_r & sY_\beta \end{bmatrix} \begin{bmatrix} \delta_{PR} \\ \delta_{PA} \\ p_g \\ r_g \\ \beta_g \end{bmatrix} \quad (20)$$

The above matrix equation is a lateral-directional mathematical model of the attacking aircraft which the pilot must control to successfully track the target. Cramer's rule (Ref 23:32) can be applied to Eq (20) to obtain the transfer functions relating the aircraft controlled variables ϕ, ψ, and β to both gust and pilot inputs. At this point, then, these equations can be used to quantitively evaluate the perturbations in ϕ, ψ, and β caused by the turbulence input and also to determine the pilot actions necessary to restore the aircraft to the nominal lead-pursuit trajectory. The numerical entries for each element of this matrix equation are listed in Appendix A, and will be substituted in the appropriate positions in the succeeding equations.

Roll Control

At this point, the attacking aircraft has been perturbed off its

nominal lead-pursuit trajectory and the pilot must generate an appropriate control to bring the pipper back on the target and consequently to return the aircraft to the nominal flight path. As discussed in the preceding chapter, the pilot's first act is to reduce roll angle error to zero by compensatory tracking in order to insure a stable lead-pursuit trajectory. Therefore, an analytic pilot model must be developed, included in the system model, and a loop closure must be made to describe the pilot's control of roll angle perturbations.

The effective time delay parameter of Eq (8) is determined by the characteristics of the disturbance input. Using Cramer's rule, the following transfer functions are derived:

$$\frac{\phi}{\eta_1} \doteq \frac{.024(s)(s+.15)(s+.50)(s+3.84)(s-3.88)\sigma_v}{(s+.19)(s+.27)^2(s^2+1.77s+1.14)(s^2+11.67s+52.80)} \qquad (21)$$

$$\frac{\phi}{\eta_2} \doteq \frac{-.0242(s+.80)(s+1.21)\sigma_w}{(s+.19)(s^2+1.77s+1.14)(s^2+11.67s+52.80)} \qquad (22)$$

Further (Ref 4:435),

$$\sigma_v = \sqrt{(L_v/L_w)}\sigma_w = 1.43\sigma_w \qquad (23)$$

where L_v is given by Eq (13), and L_w is given following Eq (10).

The symbol, $\doteq$, indicates that terms with a frequency above 20 radians/second have been replaced in the transfer function by a gain. Computations showed that this procedure altered the root mean square tracking variable errors, the primary measure of performance in this analysis, in the second or third significant digit of computation. Hence, little accuracy was sacrificed but the computations were simplified considerably by this procedure.

A log-magnitude plot, Fig. 7, shows that the dominant disturbance

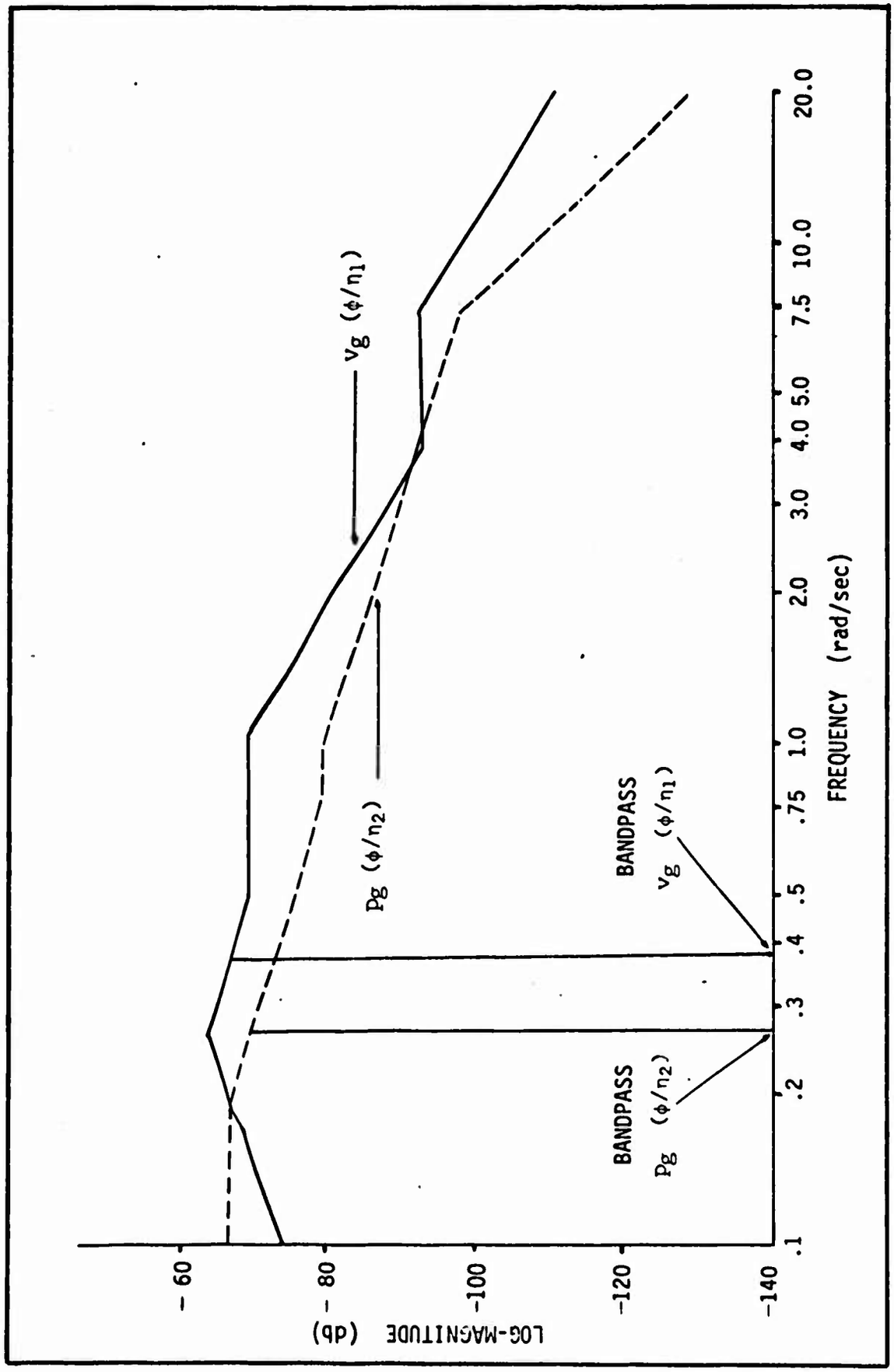

Fig. 7. Comparison of Lateral Disturbance Inputs (Roll Loop)

is determined by the pilot gain: as pilot gain is increased, the crossover frequency of the forward transfer function is raised. Since the parameters of Eq (8) are affected by the plant dynamics and the disturbance input in the region of crossover, the movement of the crossover frequency by changes in pilot gain results in alternation of the disturbance input between v_g and p_g shown in Fig. 7. In this case, the bandpass of v_g, .38 radians/second, and the bandpass of p_g, .27 radians/second, both give an effective time delay of .32 seconds and the choice of a predominant gust is probably a moot point. However, in determining the remaining parameters of Eq (8), the predominant gust input will be identified.

The next parameter of the analytic pilot model is dependent upon the characteristics of the plant. Using Cramer's rule again on Eq (20), the following transfer function is obtained:

$$\frac{\phi}{\delta_{PA}} \doteq \frac{2.54(s+.78)(s+1.25)}{(s+.19)(s^2+1.77s+1.14)} \tag{24}$$

Figure 8, a log-magnitude plot of this transfer function, shows that there is a stretch of -20 decibel/decade slope from a frequency of 1.25 radians/second to a frequency of 7.25 radians/second. This information dictates the addition of a pilot lead term at 7.25 radians/second. (Subsequent information revealed that this lead term was not necessary for stability as was originally thought. However, the term was carried through the calculations and will be included here.) At this point, two of the three required parameters have been determined and Eq (8) has the form:

$$Y_p = K_p e^{-.32j\omega}(1+s/7.25) \tag{25}$$

Using a Padé approximation for the time delay term,

$$= \frac{K_p[1-(.32/2)s](1+s/7.2)}{[1+(.32/2)s]} \tag{26}$$

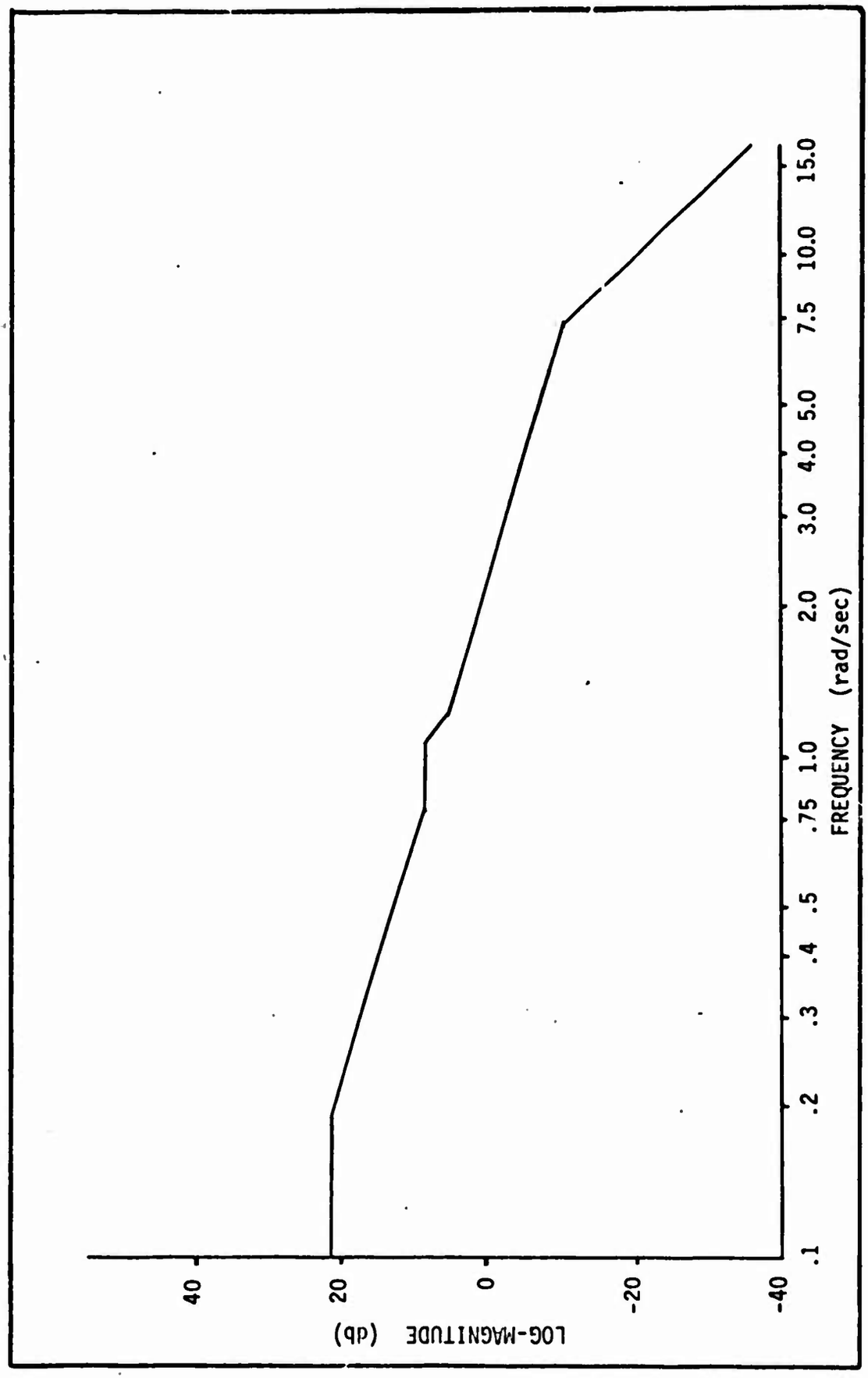

Fig. 8. Controlled Element Characteristics (Roll Loop)

$$= \frac{K_p(1 - .16s)(1 + .14s)}{(1 + .16s)} \tag{27}$$

$$= -\frac{.14K_p(s + 7.25)(s - 6.25)}{(s + 6.25)} \tag{28}$$

K_p, the pilot gain, is the only term remaining to be evaluated. McRuer states that the pilot will use gain to obtain a crossover frequency for the forward transfer function of 4.75 radians/second. To determine the appropriate gain, the following requirement holds:

$$|Y_p Y_c| = 1 \quad \text{at } \omega = 4.75 \text{ radians/second} \tag{29}$$

From Eqs (24) and (25),

$$|Y_p Y_c| = \left| \frac{(11.32)(1+1.29s)(1+.80s)(1+.13s+.01s^2)(K_p)(1-.16s)(1+.14s)}{(1+5.22s)(1+1.56s+.88s^2)(1+.22s+.02s^2)(1+.13s+.01s^2)(1+.16s)} \right|_{s=j\omega_c} = 1 \tag{30}$$

Evaluation of this equation reveals that at a frequency of 4.75 radians/second, $K_p = 1.8$ and the phase angle is -205°. Thus, the system is unstable and the pilot must operate at a lower frequency.

Since the pilot cannot operate at the desired crossover frequency, he would reduce his gain to achieve a crossover frequency with an acceptable stability margin. Thus, any pilot gain which resulted in stable operation would be acceptable.

A more appealing approach, however, is to choose a pilot gain which minimizes roll error, the pilot's primary concern at this point. The pilot is attempting to operate the closed loop system in Fig. 9, where

ϕ_T = target bank angle perturbation (assumed = 0),

ϕ = attacking aircraft bank angle,

Y_p = pilot model given by Eq (28), and

Y_c = aircraft dynamics given by Eq (24).

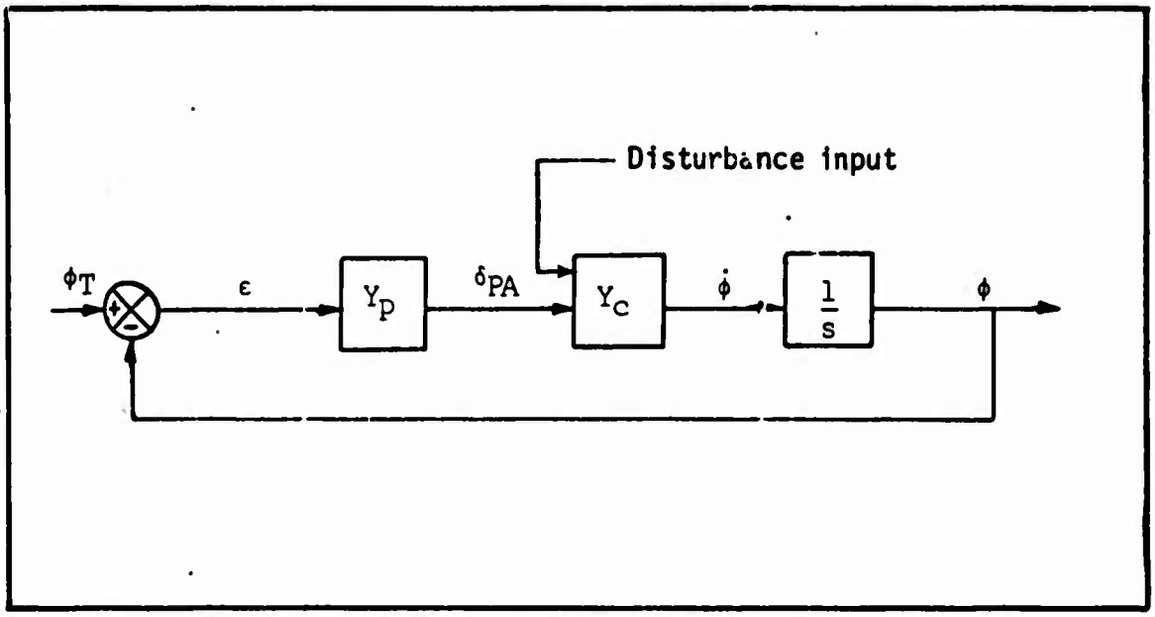

Fig. 9. Roll Angle Control System

Now,

$$\delta_{PA} = Y_p \epsilon \tag{31}$$

$$= - Y_p \dot{\phi}/s \tag{32}$$

Substituting for Y_p from Eq (28),

$$\delta_{PA} = \frac{.14K_p(s-6.25)(s+7.19)p}{(s)(s+6.25)} \tag{33}$$

Substituting this control policy into Eq (20) yields the following matrix equation:

$$\begin{bmatrix} s-L_p+ABL_{\delta_a}-AFL_{\delta_a} & -L_r-CDL_{\delta_r} & -L_\beta-CEL_{\delta_r} \\ -N_p+ABN_{\delta_a}-AFN_{\delta_a} & s-N_r-CDN_{\delta_r} & -N_\beta-CEN_{\delta_r} \\ -sY_p-Y_\phi+ABY_{\delta_a}s-AFY_{\delta_a}s & -sY_r-Y_\phi-CDY_{\delta_r}s & s^2-sY_\beta-CEY_{\delta_r}s \end{bmatrix} \begin{bmatrix} p \\ r \\ \beta \end{bmatrix}$$

$$= \begin{bmatrix} CL_{\delta_r} & AL_{\delta_a} & L_p & L_r & L_\beta \\ CN_{\delta_r} & AN_{\delta_a} & N_p & N_r & N_\beta \\ CY_{\delta_r}s & AY_{\delta_a}s & sY_p & sY_r & sY_\beta \end{bmatrix} \begin{bmatrix} \delta_{PR} \\ \delta_{PA} \\ p_g \\ r_g \\ \beta_g \end{bmatrix} \tag{34}$$

where terms A through E are given in Appendix A, and

$$F = \frac{.14K_p(s-6.25)(s+7.14)}{(s)(s+6.25)} \tag{35}$$

Equation (34) represents the closed loop dynamics of the control system given in Fig. 9. The optimal pilot gain, $K_p = .7$, was determined by varying K_p in Eq (34) from .1 to 1.0, and then, for each pilot gain, determining Eqs (38) and (39) and evaluating Eqs (42) and (43). Figure 10 is a graph of the data for p_g and v_g. This plot presents data for K_p vs K_w and K_p vs K_v where

$$\sigma_{\phi_v} = K_v\sigma_v \tag{36}$$

$$\sigma_{\phi_w} = K_w\sigma_w \tag{37}$$

Using Cramer's rule, the following transfer functions are obtained using a pilot gain of .7 ($K_p = .7$ in Eq (35)):

$$\frac{\phi}{n_1} \doteq \frac{.00251(s)(s+.15)(s+.50)(s+3.84)(s-3.88)}{(s+.27)^2(s+.64)(s+1.74)(s^2+2.47s+9.55)} \tag{38}$$

$$\frac{\phi}{n_2} \doteq \frac{-.002527(s+.80)(s+1.21)}{(s+.64)(s+1.74)(s^2+2.47s+9.55)} \tag{39}$$

These equations relate the roll angle output to the two disturbance inputs; since the predominant disturbance has not been identified, the effect of both gust inputs must be evaluated.

The pilot adjusts his gain to minimize the roll angle perturbations resulting from the turbulence inputs. Since the gust inputs are represented by two uncorrelated white noise signals of unity spectrum, the spectral densities of ϕ/n_1 and ϕ/n_2 are

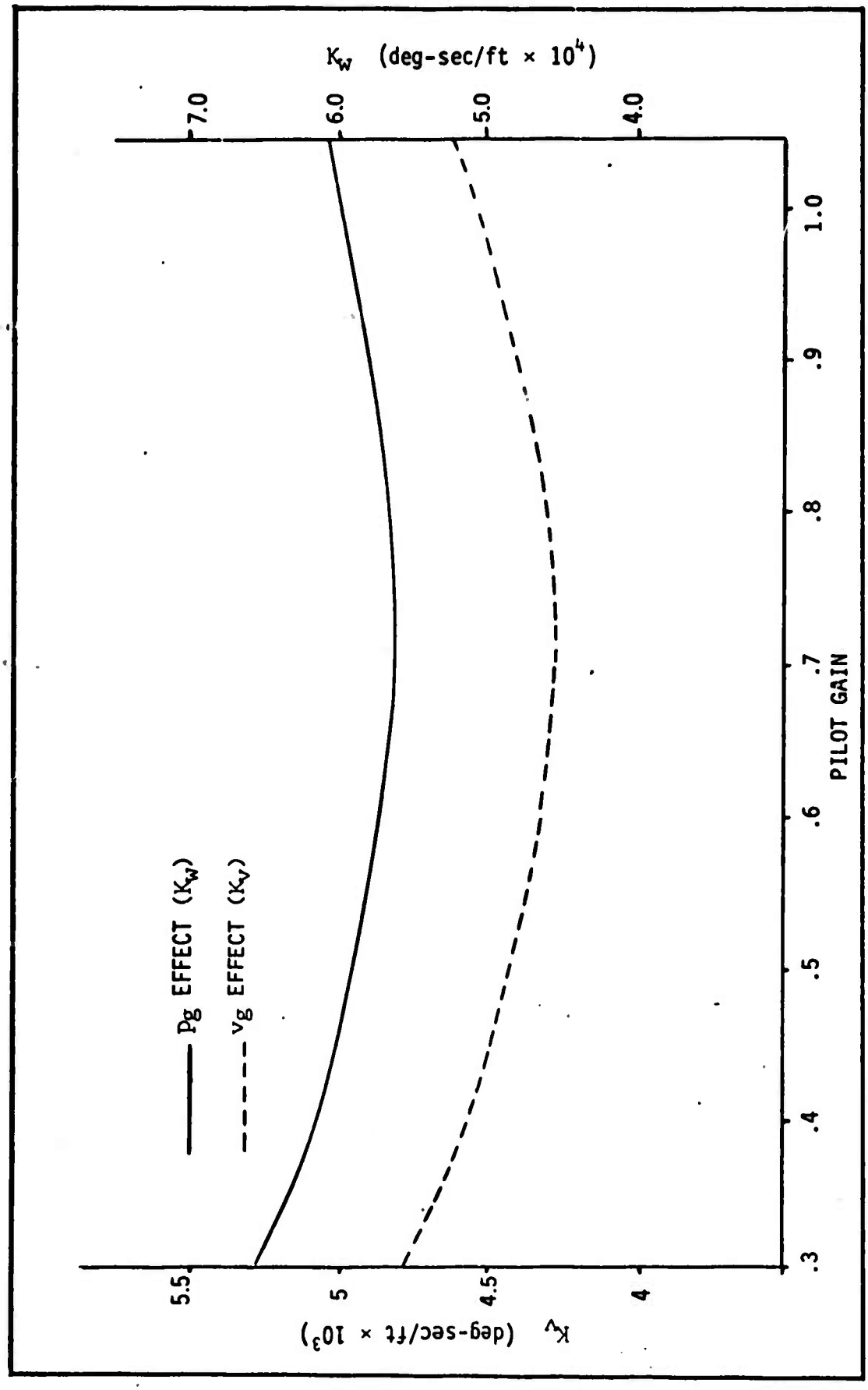

Fig. 10. Roll Angle Perturbation vs Pilot Gain

$$\Phi_{\eta_1\eta_1}(\omega) = \frac{\phi(j\omega)}{\eta_1} \cdot \frac{\phi(-j\omega)}{\eta_1} \tag{40}$$

$$\Phi_{\eta_2\eta_2}(\omega) = \frac{\phi(j\omega)}{\eta_2} \cdot \frac{\phi(-j\omega)}{\eta_2} \tag{41}$$

The root mean square values of these perturbation power spectra are

$$\sigma_{\phi_v} = \sqrt{\left[\int_0^\infty \Phi_{\eta_1\eta_1}(\omega)\, d\omega\right]} = .00428\sigma_v, \text{ for Eq (36)} \tag{42}$$

$$\sigma_{\phi_w} = \sqrt{\left[\int_0^\infty \Phi_{\eta_2\eta_2}(\omega)\, d\omega\right]} = .000570\ \sigma_w \text{ for Eq (37)} \tag{43}$$

Integral (43) was evaluated using a standard fifth order integral equation (Ref 21:4-73); integral (42) was not of the proper form and it was evaluated using a method based on Simpson's rule (Ref 5:2-114).

A log-magnitude plot (Fig. 11) of the forward transfer function reveals that for $K_p = .7$, the crossover frequency is 2.0 radians/second with a phase angle of -135°. Thus the system is stable; the pilot has a phase margin of 45°. Further, Fig. 8, page 31, shows that at a frequency of 2.0 radians/second, the plant has a slope of -20 decibel/decade and, consequently, Eq (9) is satisfied. Also, at a frequency of 2.0 radians/second, Fig. 7, page 29, reveals that v_g is the primary disturbance; this is confirmed by Fig. 10, page 35, which shows K_v to be an order of magnitude greater than K_w. Finally, the complete roll pilot model is

$$Y_p = \frac{-.0973(s + 7.25)(s - 6.25)}{(s + 6.25)} \tag{44}$$

The development of this pilot model has been explained in great detail and illustrates the procedure which will be applied in the lateral and longitudinal compensatory tracking tasks. Therefore, the parameters for these two remaining pilot models will not be derived in detail.

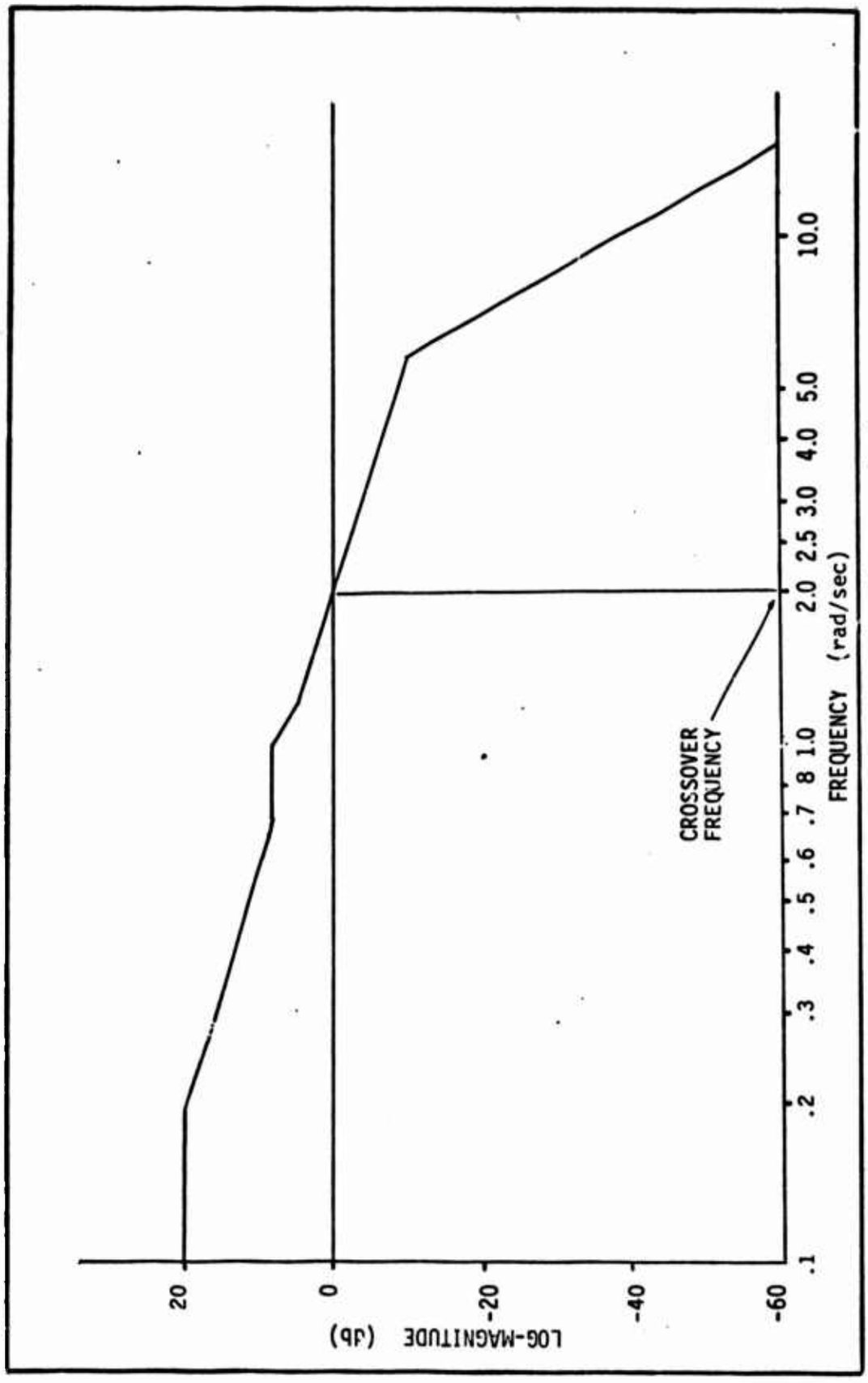

Fig. 11. Forward Transfer Function Characteristics (Roll Loop)

Lateral Tracking

The pilot has now matched the roll angle of the target and thus has insured a stable lead-pursuit trajectory. The gust disturbances, however, introduce yaw rate perturbations which also cause the pipper to be displaced laterally from the target. Therefore, the pilot generates another aileron command to zero the lateral tracking error μ. Again, this is a compensatory tracking task and an analytic pilot model must be developed for this case.

The pilot observes the following perturbation errors:

$$\frac{\mu}{\eta_1} = \frac{\psi - (.03516)\phi}{\eta_1} \tag{45}$$

$$\frac{\mu}{\eta_2} = \frac{\psi - (.03516)\phi}{\eta_2} \tag{46}$$

where ψ/η_1, ϕ/η_1, ψ/η_2, ϕ/η_2 are determined from Eq (34) using Cramer's rule, and

$$\mu = \psi - (.03516)\phi \tag{47}$$

is developed by substituting Σ and α_0 determined in Chapter IV, page 69, into Eq (7), Chapter II.

Substituting the appropriate values,

$$\frac{\mu}{\eta_1} \doteq \frac{.07948(s + .15)(s + .19)(s + .5)(s^2 + 2.98s + 3.12)}{(s + .27)^2(s + .64)(s + 1.74)(s^2 + 2.47s + 9.55)} \tag{48}$$

$$\frac{\mu}{\eta_2} \doteq \frac{.01325(s - .14)(s + .52)}{(s)(s + .64)(s + 1.74)(s^2 + 2.47s + 9.55)} \tag{49}$$

A Bode plot of these two equations, Fig. 12, reveals that v_g is the dominant gust with a bandwidth of 8.0 radians/second. This requires that the effective time delay be approximately .12 seconds.

The plant operating characteristics are

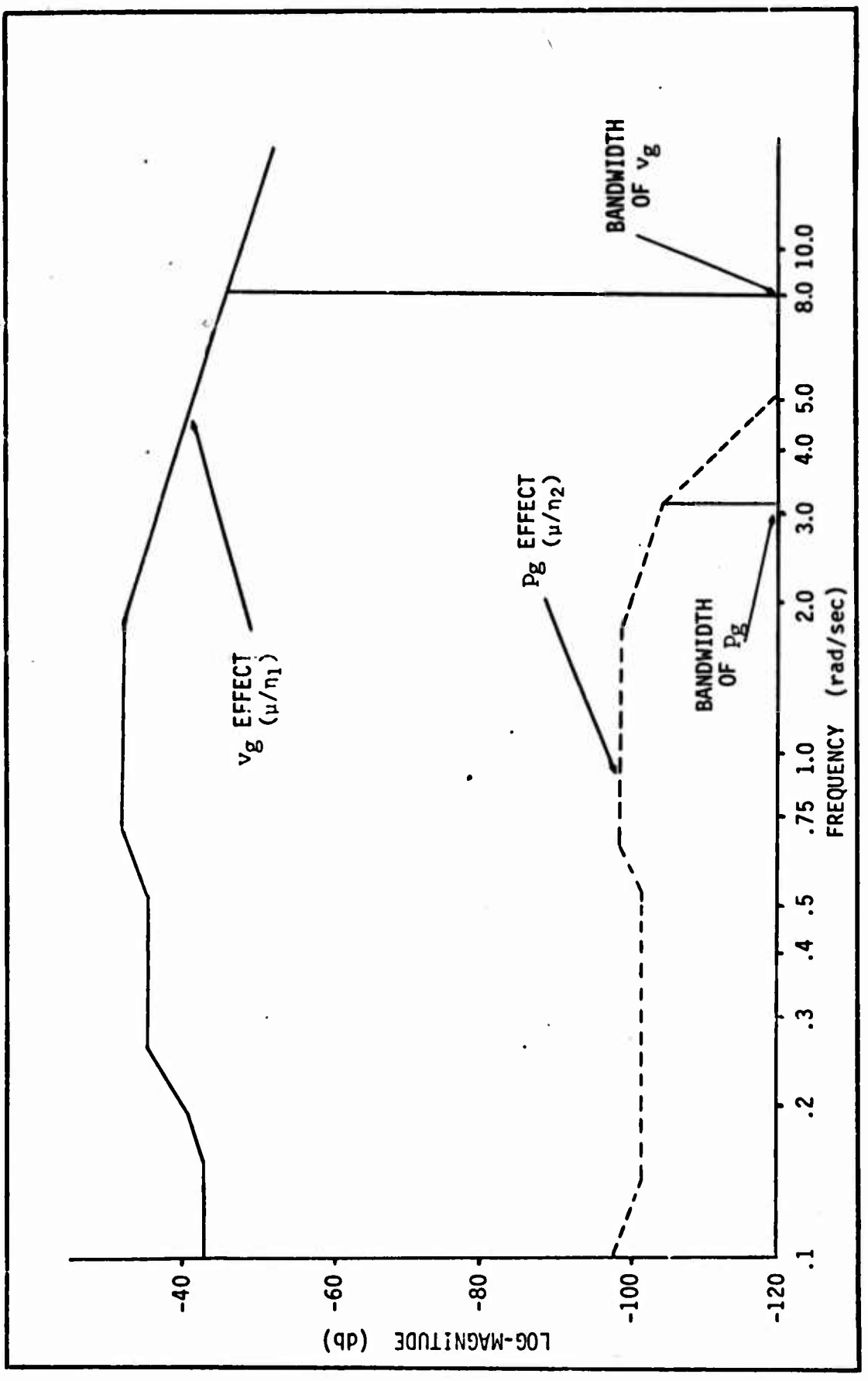

Fig. 12. Comparison of Lateral Disturbance Inputs (Tracking Loop)

$$\frac{\mu}{\delta_{PA}} = \frac{\psi - .03516\phi}{\delta_{PA}} \tag{50}$$

Determining the appropriate transfer functions from Eq (34) and substituting into Eq (50) yields

$$\frac{\mu}{\delta_{PA}} \doteq \frac{-.2883(s-.33)(s+.47)(s+6.25)}{(s)(s+.64)(s+1.74)(s^2+2.47s+9.55)} \tag{51}$$

A Bode plot of this transfer function shows a -20 decibel/decade slope from $\omega = 0$ to $\omega = .32$. Operation above this range of frequency is prohibited by the stability limits of the plant.

The disturbance input bandwidth and the plant dynamics given by Eqs (48) and (51), respectively, dictate the following pilot model form:

$$Y_p = \frac{-K_p(s-16.66)}{(s+16.66)} \tag{52}$$

As in the preceding case, K_p, the pilot gain, is selected to minimize closed loop tracking error. The tracking loop model is shown in Fig. 13.

The control law is

$$\delta_{PA} \doteq \left(\frac{+K_p(s-16.6)}{(s+16.6)}\right)\left(\frac{\dot{\psi} - (\Sigma - \alpha_0)\dot{\phi}}{s}\right)$$

$$\doteq Q\dot{\psi} - R\dot{\phi} \tag{53}$$

where

$$Q = \frac{K_p(s-16.6)}{(s)(s+16.6)} \tag{54}$$

$$R = \frac{K_p(s-16.6)}{(s)(s+16.6)}(\Sigma - \alpha_0) \tag{55}$$

Substituting Eq (53) into Eq (34), the following matrix equation is generated:

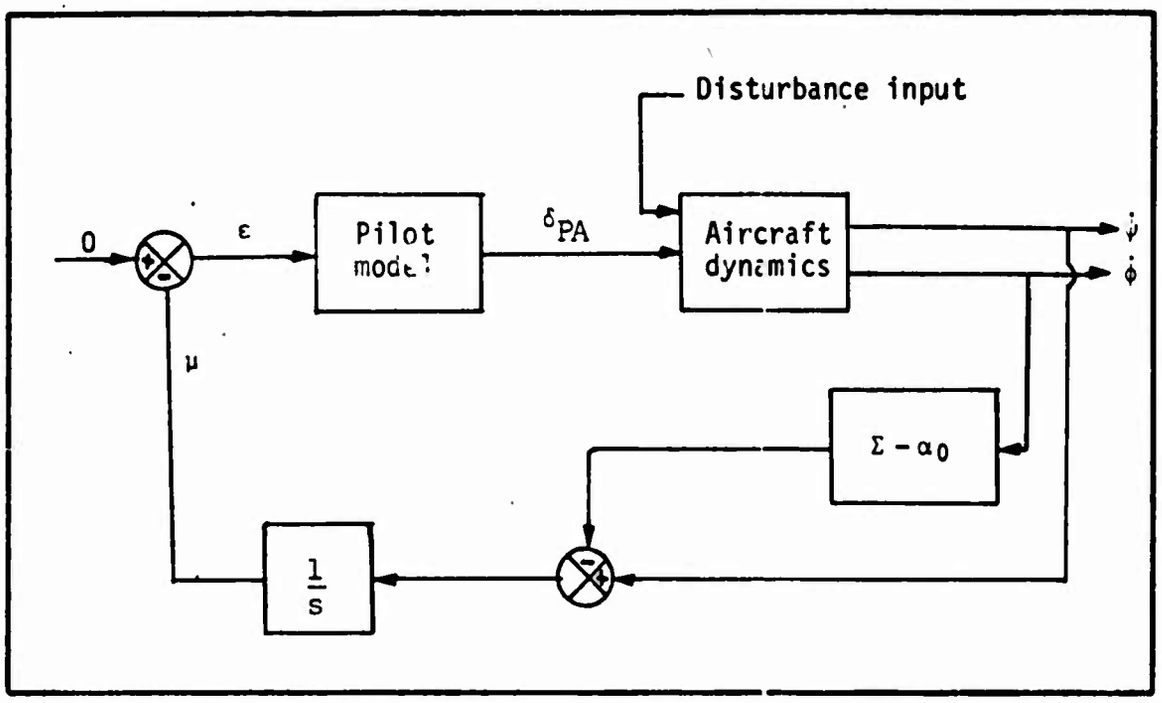

Fig. 13. Lateral Tracking Control System

$$\begin{bmatrix} s-L_p+ABL_{\delta_a}-AFL_{\delta_a}+ARL_{\delta_a} & -L_r-CDL_{\delta_r}-QAL_{\delta_a} & -L_\beta-CEL_{\delta_r} \\ -N_p+ABN_{\delta_a}-AFN_{\delta_a}+ARN_{\delta_a} & s-N_r-CDN_{\delta_r}-QAN_{\delta_a} & -N_\beta-CEN_{\delta_r} \\ -sY_p-Y_\phi+ABY_{\delta_r}s-AFY_{\delta_a}s+ARY_{\delta_a}s & sY_r-Y_\phi-CDY_{\delta_r}s-QAY_{\delta_a}s & s^2-sY_\beta-CEY_{\delta_r}s \end{bmatrix} \begin{bmatrix} p \\ r \\ \beta \end{bmatrix}$$

$$= \begin{bmatrix} CL_{\delta_r} & AL_{\delta_a} & L_p & L_r & L_\beta \\ CN_{\delta_r} & AN_{\delta_a} & N_p & N_r & N_\beta \\ CY_{\delta_r}s & AY_{\delta_a}s & sY_p & sY_r & sY_\beta \end{bmatrix} \begin{bmatrix} \delta_{PR} \\ \delta_{PA} \\ p_g \\ r_g \\ \beta_g \end{bmatrix} \qquad (56)$$

where terms A through E and the appropriate stability derivatives are given in Appendix A, term F is given in Eq (35), and terms Q and R are given by Eqs (54) and (55), respectively.

As in the roll angle control task, Cramer's rule is applied to Eq (56)

to determine the closed loop determinant and the transfer functions relating yaw rate and roll rate outputs to the disturbance input. From these relationships, an equation relating μ, the tracking variable, to the disturbance input is developed. The pilot gain, K_p, is then iterated from .1 to 1.0 in this equation to determine the gain yielding minimum tracking error. This process reveals that $K_p = .1$ minimizes the rms intensity of the tracking response to a disturbance input.

Now, at a pilot gain $K_p = .1$, the pilot model is

$$Y_p = \frac{-.1(s - 16.66)}{(s + 16.66)} \tag{57}$$

The forward transfer function of the system depicted in Fig. 13 is obtained by combining Eqs (51) and (57):

$$\frac{\mu}{\varepsilon} \doteq \frac{.0297(s - .32)(s + .47)(s + 6.25)}{(s)(s + .64)(s + 1.74)(s^2 + 2.47s + 9.55)} \tag{58}$$

A Bode plot of Eq (58) reveals that the crossover frequency is .0004 radians/second. Thus, the pilot is operating on a -20 decibel/decade slope of the plant and, consequently, the analytic pilot model is valid as it meets all constraints.

The closed loop system depicted in Fig. 13, and mathematically described by Eq (56), including the pilot model given by Eq (57), has the following response characteristics:

$$\frac{\mu}{\eta_1} \doteq \frac{-.00306(s + .15)(s + .19)(s + .5)(s^2 + 2.99s + 9.09)}{(s + .27)^2(s + .64)(s + 1.74)(s^2 + 2.48s + 9.51)} \tag{59}$$

$$\frac{\psi}{\eta_1} \doteq \frac{-.00297(s + .5)(s + .15)(s + .18)(s^2 + 3.11s + 9.84)}{(s + .27)^2(s + .64)(s + 1.74)(s^2 + 2.48s + 9.51)} \tag{60}$$

$$\frac{\phi}{\eta_1} \doteq \frac{+.00252(s - .001)(s + .15)(s + .5)(s + 3.81)(s - 3.88)}{(s + .27)^2(s + .64)(s + 1.74)(s^2 + 2.48s + 9.51)} \tag{61}$$

$$\frac{\beta}{n_1} \doteq \frac{+.00357(s+.15)(s^2+.77s+.16)(s^2+3.1s+9.86)}{(s+.27)^2(s+.64)(s+1.74)(s^2+2.48s+9.51)} \quad (62)$$

These four equations describe the propagation of disturbance inputs through the system dynamics to the aircraft controlled variables. Thus, they are powerful analytic tools in that they allow us to quantitively evaluate variations in μ, the tracking variable, and ϕ, ψ, and β, the aircraft controlled variables caused by a specific gust input.

Since the disturbance is a random variable in this study, it must be dealt with in a statistical sense. The approach, as demonstrated in determining the pilot gains in the two analytical pilot models, is to integrate the power spectrum densities of the filters represented by Eqs (59) through (62) and then to relate the variance of the output to the variance of the input.

Accomplishing this for the example firing situation yields

$$\sigma_\mu = .1406^{\circ} \quad \sigma_v \quad (63)$$

$$\sigma_\phi = .2452 \quad \sigma_v \quad (64)$$

$$\sigma_\psi = .1429 \quad \sigma_v \quad (65)$$

$$\sigma_\beta = .1759 \quad \sigma_v \quad (66)$$

Next, the magnitude of σ_v needs to be determined. From Chalk (Ref 4:440-443) the expected value of rms vertical gust intensity is

$$\sigma_w = 3.252\sqrt{(P_1)} \quad (67)$$

where

P_1 = probability of encountering turbulence at 15,000 ft

= .09 (from Fig. 3, page 443, Ref 4)

$$\sigma_w = .975 \text{ ft/sec} \quad (68)$$

Also, Eq (23) relates σ_v and σ_w; thus,

$$\sigma_v = 1.39 \quad \text{ft/sec} \tag{69}$$

Substituting Eq (69) into Eqs (63) through (66) yields

$$\sigma_\mu = .1960° \tag{70}$$

$$\sigma_\phi = .3418° \tag{71}$$

$$\sigma_\psi = .1992° \tag{72}$$

$$\sigma_\beta = .2452° \tag{73}$$

One final task must be accomplished to complete the model. Fig. 4, page 22, indicates that remnant must be added to the linear element of the pilot response to completely duplicate the pilot's performance. Remnant, which is defined as the portion of the pilot's control output power which is not linearly correlated with the system input, contributes a relatively large portion of the pilot's response in a task such as the example firing situation (Ref 16:131). Levison has successfully represented remnant as an equivalent observation noise source (Ref 9). For a scalar observation, his model has the simple structure:

$$\sigma_R^2 = P^2(\sigma_m^2 + \sigma^2) \tag{74}$$

where

σ_R^2 = variance of remnant injected entirely as an equivalent visual noise source,

P = constant noise ratio independent of system dynamics and input signal bandwidth,

σ^2 = variance of displayed signal, and

σ_m^2 = variance of a noise source accounting for the minimum or threshold level of remnant.

Thus, the lateral tracking error, μ, should be revised to account for the effect of pilot remnant.

$$\sigma_\mu^2 = \sigma_{\mu_I}^2 + \sigma_{\mu_R}^2 \tag{75}$$

where

$\sigma^2_{\mu_I}$ = input correlated variance, and

$\sigma^2_{\mu_R}$ = remnant induced variance.

$$\sigma^2_\mu = \sigma^2_{\mu_I} + P^2(\sigma^2_m + \sigma^2_\mu) \tag{76}$$

$$= (1 + P^2)\sigma^2_\mu + P^2\sigma^2_m \tag{77}$$

For the F-4E (Ref 16:132),

$$P = 1.72$$

$$\sigma_m = .065°$$

Substituting Eqs (70) through (73) into Eq (77) yields

$$\sigma_\mu = \sqrt{[(1+(1.72)^2)(.19598)^2 + (1.72)^2(.065)^2]} \tag{78}$$

$$= .4057° \tag{79}$$

$$\sigma_\phi = .6894° \tag{80}$$

$$\sigma_\psi = .4119° \tag{81}$$

$$\sigma_\beta = .5007° \tag{82}$$

At this point, a model relating disturbance input to the output of the aircraft controlled variables has been developed and applied to the example firing situation. This represents accomplishment of the first objective of this chapter; now, a similar model must be developed for the longitudinal case.

Longitudinal Input and Controlled Element

The vertical turbulence spectrum, which induced a roll rate in the lateral case, also disturbs the aircraft aerodynamically in the longitudinal axis. This vertical gust, w_g, produces angle of attack, pitch rate, and angle of attack rate perturbations which are observed by the pilot as disturbances in the pitch attitude of the aircraft. Thus, when the attacking

aircraft is perturbed from its nominal lead-pursuit trajectory, the pilot observes vertical displacement of the pipper from the target aircraft as well as the lateral pipper displacement discussed in the previous section.

As in the lateral case, the vertical gust, w_g, can be modeled by passing a Gaussian random "white" noise signal through a low-pass filter (Ref 4:460-461). The filter characteristics can be modeled as shown in Fig. 14, where

$$T_{wg} = \frac{\sqrt{(L_w/\pi U_0)}[1 + \sqrt{(3)}L_w s/U_0]\sigma_w}{(1 + L_w s/U_0)^2} \tag{83}$$

η_3 = white noise signal,

$$T_{\dot{\theta}g} = \frac{s/U_0}{[1 + (4b/\pi U_0)s]} \tag{84}$$

U_0, L_w, and b are given after Eq (3).

Substituting the appropriate values for the example firing situation into Eqs (83) and (84) yields

$$\frac{\alpha_g}{\eta_3} = \frac{-.0007572(s + .31)\sigma_w}{(s + .54)^2} \tag{85}$$

$$\frac{\dot{\alpha}_g}{\eta_3} = \frac{-.01473(s^2 + .31s)\sigma_w}{(s + .54)^2(s + 19.46)} \tag{86}$$

$$\frac{\dot{\theta}_g}{\eta_3} = \frac{.01473(s^2 + .31s)\sigma_w}{(s + .54)^2(s + 19.46)} \tag{87}$$

The approximate equations of aircraft longitudinal motion, the "short period" equations, describe a portion of the controlled element as well as additional filtering for the gust input. Hence, these equations relate the aircraft longitudinal response to elevator and vertical gust inputs (Ref 1:32):

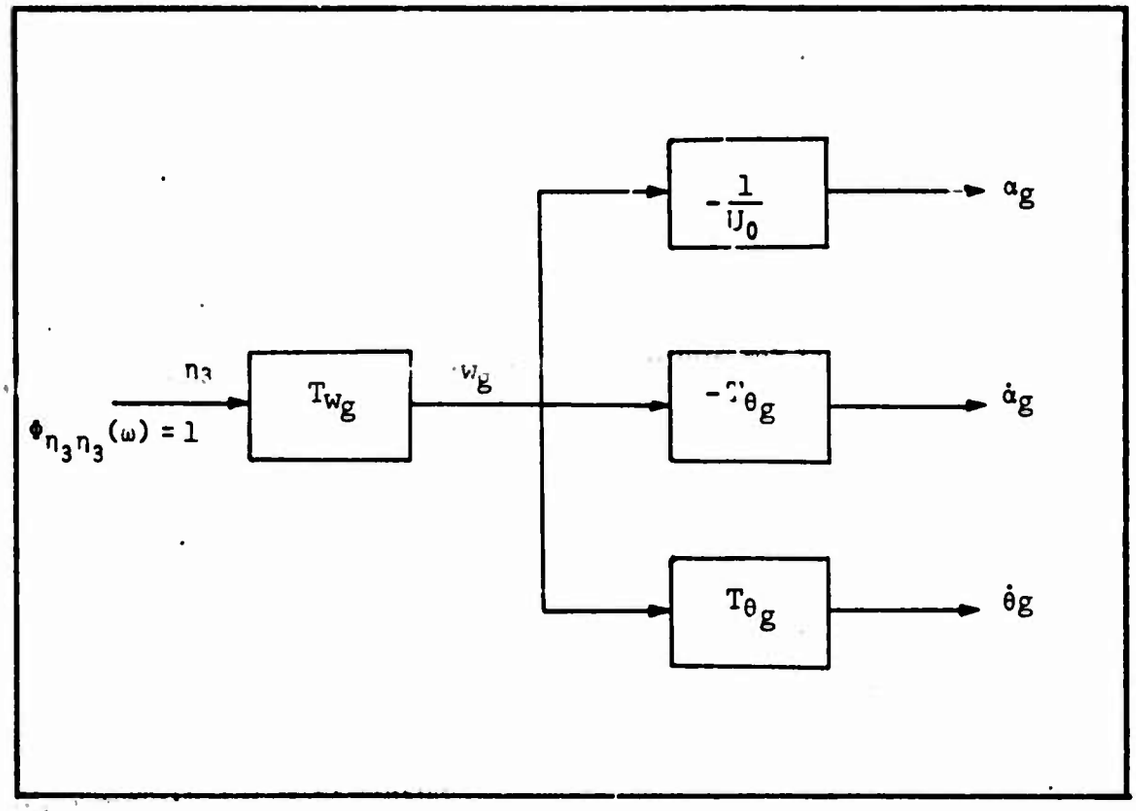

Fig. 14. Model of the Effect of Vertical Gusts on the Longitudinal Dynamics of an Aircraft (Adapted from Ref 17:76)

$$\begin{bmatrix} s-M_{\dot{\theta}} & -M_{\dot{\alpha}}s-M_{\alpha} \\ -1-Z_{\dot{\theta}} & s-Z_{\alpha} \end{bmatrix} \begin{bmatrix} \dot{\theta} \\ \Delta\alpha \end{bmatrix} = \begin{bmatrix} M_{\delta} & M_{\dot{\theta}} & M_{\alpha} & M_{\dot{\alpha}} \\ Z_{\delta} & Z_{\dot{\theta}} & Z_{\alpha} & 0 \end{bmatrix} \begin{bmatrix} \delta \\ \dot{\theta}_g \\ \alpha_g \\ \dot{\alpha}_g \end{bmatrix} \tag{88}$$

The aircraft dynamics are altered by the stability augmentation system (SAS) incorporated in the pitch channel and hence the effects of the pitch SAS must be included in Eq (88).

The pitch axis control system can be represented as (Ref 17:155)

$$\delta(s) = G_p(s)[K(s)\delta_{PE}(s) + H_p(s)\dot{\theta}(s)] \tag{89}$$

where

$\delta(s)$ = elevator deflection,

$G_p(s)$ = power cylinder dynamics,

$K(s)$ = linkage dynamics,

$\delta_{PE}(s)$ = longitudinal control stick deflection, and

$H_p(s)$ = pitch rate feedback dynamics.

Substituting Eq (39) into Eq (88) yields

$$\begin{bmatrix} s-M_{\dot\theta}-M_\delta GH & -M_{\dot\alpha}s-M_\alpha \\ -1-Z_{\dot\theta}-Z_\delta GH & s-Z_\alpha \end{bmatrix} \begin{bmatrix} \dot\theta \\ \Delta\alpha \end{bmatrix} = \begin{bmatrix} M_\delta GK & M_{\dot\theta} & M_\alpha & M_{\dot\alpha} \\ Z_\delta GK & Z_{\dot\theta} & Z_\alpha & 0 \end{bmatrix} \begin{bmatrix} \delta_{PE} \\ \dot\theta_g \\ \alpha_g \\ \dot\alpha_g \end{bmatrix} \qquad (90)$$

The above matrix equation is a mathematical model of the longitudinal axis of the attacking aircraft which the pilot must control to successfully track the target. Cramer's rule can be applied to Eq (90) to obtain transfer functions relating the aircraft controlled variables, $\dot\theta$ and $\Delta\alpha$, to both gust and pilot inputs. These equations can be used to quantitively evaluate the perturbations in $\dot\theta$ and $\Delta\alpha$ caused by the turbulence input and also to determine the pilot's actions necessary to restore the aircraft to the nominal lead-pursuit trajectory. The numerical entries for each element of this matrix equation are listed in Appendix A and will be substituted in the appropriate positions in the succeeding equations.

Longitudinal Tracking

The attacking aircraft has been perturbed from its nominal lead-pursuit trajectory by gust inputs; the pilot observes this perturbation as both lateral and longitudinal displacement of the pipper from the target. In the preceding sections, a model has been developed to describe pilot control

of lateral pipper displacement; a similar model will now be developed to account for control of longitudinal pipper displacement by the pilot.

As discussed in Chapter II, the pilot controls θ, the angle in the pitch axis between the pipper and the target, which is generated by the gust input. Thus, the pilot is confronted with a third compensatory tracking task. This requires the development of another analytical pilot model, substitution of this model into the system, and a loop closure to control the pitch tracking variable θ.

The closed loop system describing the longitudinal tracking task is shown in Fig. 15.

Before proceeding, it is necessary to determine the transfer function relating $\dot{\theta}$, the aircraft pitch rate, to θ_p, the pipper position on the combining glass. The equations describing the dynamics of the fire control system, including the sight, are (Ref 15:17-19)

$$\frac{\theta_p}{\dot{\theta}} = \frac{as^2 + bs + c}{s(s + \Delta V/D)(T_f s + 1)} \tag{91}$$

where

$\dot{\theta}$ = pitch rate of the aircraft,

θ_p = depression of pipper below zero depression line,

$$\Delta V = V_T - V_A \tag{92}$$

with V_A = attacking aircraft velocity

V_T = target aircraft velocity

D = target present range,

T_f = time of flight of projectile,

$$a = (1 + WT_f) \tag{93}$$

$$b = (\Delta V/D)(1 - WT_f + Z_\alpha T_f) - Z_\alpha(1 + V_T T_f/D) \tag{94}$$

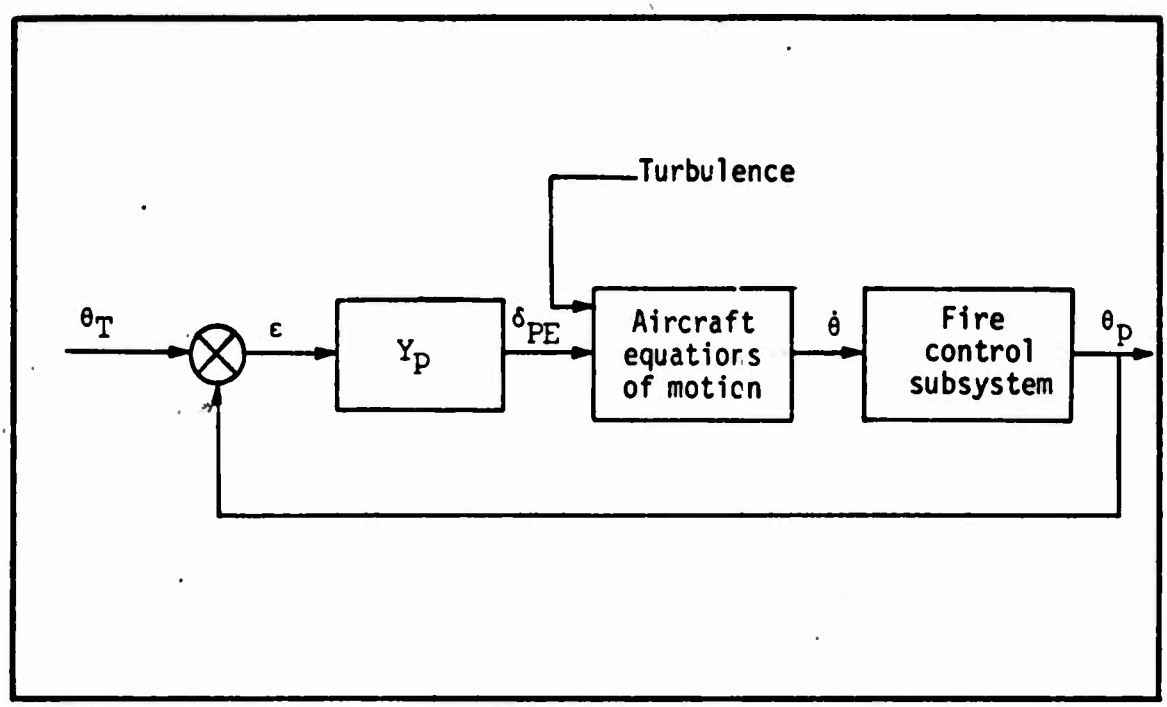

Fig. 15. Longitudinal Tracking System

$$c = - Z_\alpha V_T/D \ * \tag{95}$$

$$W = - (V_A/DV_f)(Z_\alpha + 2J_V/T_f) \tag{96}$$

The aerodynamic constants required in these equations are found in Appendix A; the firing situation parameters and ballistic solution data are found in Chapter IV. Substituting the appropriate values results in the following equation:

$$\frac{\theta_p}{\dot{\theta}} = \frac{.825(s + .47)(s + 1.65)}{(s)(s + 1.32)(s - .053)} \tag{97}$$

Applying Cramer's rule to Eq (90) to determine the transfer function $\dot{\theta}/n_3$ and combining this equation and Eq (97) yields Eq (98), which describes the perturbation observed by the pilot:

---

*In the referenced technical report, Eq (95) is preceded by a positive, not by a negative sign as in this report. The sign change was made for two reasons. A negative sign coupled with a negative Z_α results in a numerically positive term which is required for stability. Second, when the contractor's data was substituted into his equations, a numerically positive term occurs in his following equations. This can only occur if Z_α is positive or if both the term and Z_α are negative.

$$\frac{\theta_p}{\eta_3} \doteq \frac{.009955(s+.31)(s+.47)(s+1.65)}{(s-.053)(s+.54)^2(s+1.32)(s^2+7.28s+18.10)} \tag{98}$$

A Bode plot of this transfer function shows the input bandwidth to be .05 radian/second.

The plant transfer function is

$$\frac{\theta_p}{\delta_{PE}} \doteq \frac{19.8422(s+.47)(s+.98)(s+1.65)}{(s)(s-.053)(s+1.32)(s^2+7.28s+18.10)} \tag{99}$$

A Bode plot of Eq (99) indicates that the pilot would add a lag at 1 radian/second in order to obtain a -20 decibel/decade slope from .47 rad/sec to 1.32 rad/sec and from 1.65 rad/sec to 4.25 rad/sec.

From the information contained in Eqs (98) and (99), Eq (8) becomes

$$Y_p = \frac{-K_p(s-6.25)}{(s+1)(s+6.25)} \tag{100}$$

The pilot will select his gain to minimize pitch tracking error. As in the lateral case, the optimum pilot gain, K_p, is selected by closing the tracking loop and iterating K_p to determine the minimum root mean square tracking error.

Thus the control law for the system depicted in Fig. 15 is

$$\delta_{PE} = \frac{.825K_p(s-6.25)(s+.47)(s+1.65)\dot{\theta}}{(s)(s+1.32)(s-.053)(s+1)(s+6.25)} \tag{101}$$

Iterating pilot gain in Eq (101) from .1 to 1.0, the optimal gain is determined to be $K_p = .4$. Substituting Eq (101) into Eq (90) and applying Cramer's rule, we have, for $K_p = .4$,

$$\frac{\theta_p}{\eta_3} \doteq \frac{.03725(s)(s-.05)(s+.31)(s+1)(s+1.32)}{(s+.54)^2(s^2+.28s+.40)(s^2+2.02s+1.03)(s+2.91)} \tag{102}$$

For this gain, the rms tracking error is

$$\sigma_\theta = .08855\sigma_w = .0863^\circ \tag{103}$$

Adding pilot remnant,

$$\sigma_\theta = .1850^\circ \tag{104}$$

To determine the operating frequency of the closed loop system, the crossover frequency of the forward transfer function must be determined. The forward transfer function, with pilot gain, K_p, unspecified, is a combination of Eqs (99) and (100),

$$\frac{\theta_p}{\epsilon} \doteq \frac{19.8422(s+.47)(s+1.65)(s-6.25)(K_p)}{(s)(s-.053)(s+1.32)(s^2+7.28s+18.10)(s+6.25)} \tag{105}$$

A Bode plot of Eq (105), Fig. 16, with $K_p = .4$, reveals that the pilot is operating where the system slope is -40 decibels/decade. This is an unacceptable operating point, even though tracking error is at a minimum. Equation (99) indicated that a slope of -20 decibels/decade exists in the frequency range of .47 to 1.32 radians/second. The Bode plot of Eq (105) reveals that a pilot gain $K_p = .8$ will give a crossover frequency of .90 radians/second. This is exactly in the middle of the -20 decibels/decade slope and hence acceptable to the pilot as an operating point.

For $K_p = .8$, Eq (102) becomes

$$\frac{\theta_p}{n_3} \doteq \frac{.001668(s)(s-.05)(s+.31)(s+1)(s+1.32)}{(s+.54)(s+.72)(s+.95)(s+2.02)(s^2+.23s+1.22)} \tag{106}$$

Integration of this equation and addition of pilot remnant results in the following root mean square tracking error:

$$\sigma_\theta = .2482^\circ \tag{107}$$

Similarly,

$$\sigma_{\Delta\alpha} = .2112^\circ \tag{108}$$

Thus, in securing an acceptable operating regime, mean square tracking

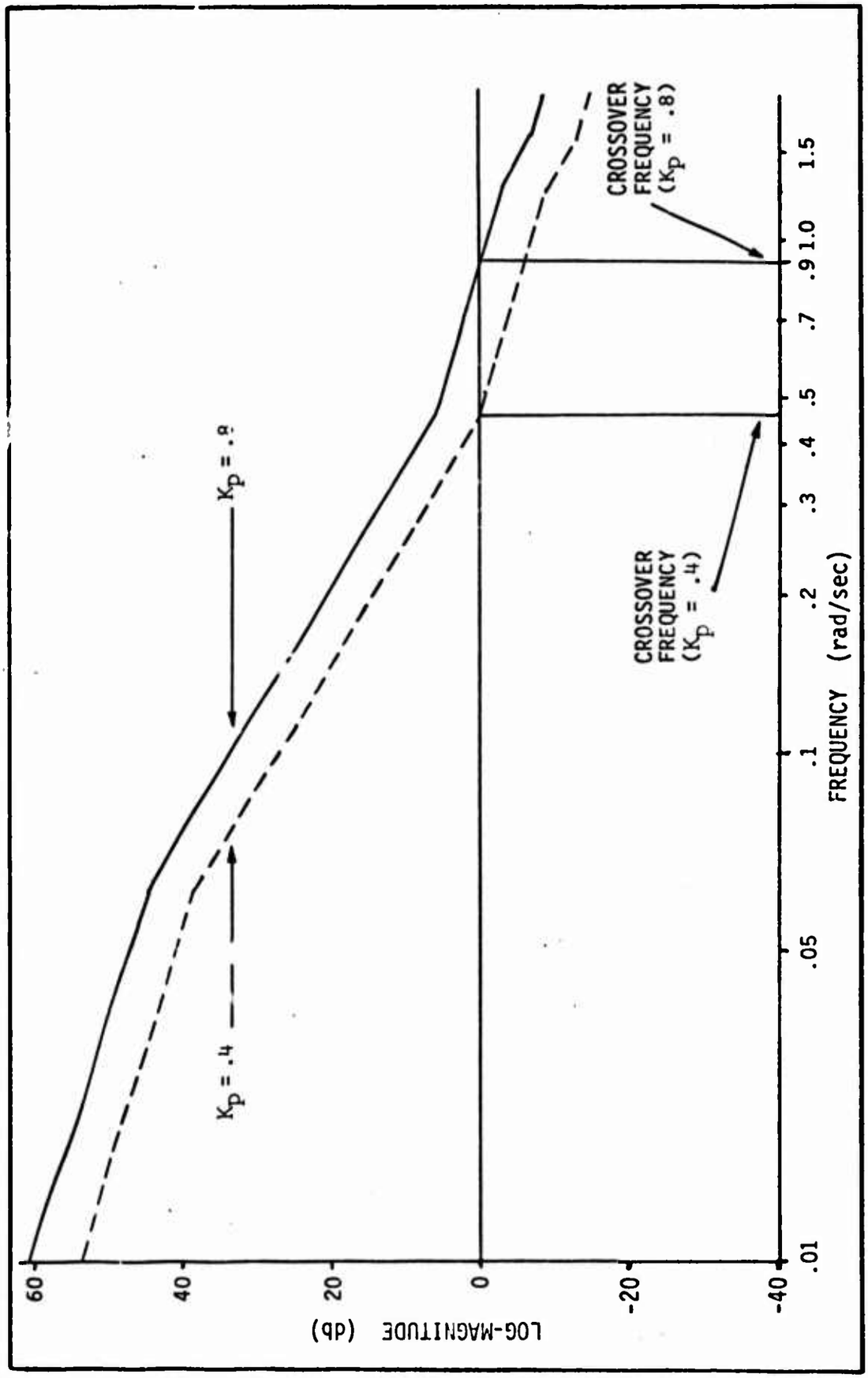

Fig. 16. System Crossover Frequency vs Pilot Gain

error has risen considerably from Eq (104) to Eq (107).

Equation (106) represents completion of the second model; it is a mathematical statement which relates pitch tracking error, θ, to the gust input when the pilot is attempting to return the pipper to the target and hence reduce tracking error to zero.

To this point, the lateral case and the longitudinal case have been dealt with as separate entities. However, only one pilot controls both of these channels and, hence, the interdependence of these two tasks must be considered.

Homogeneous Pilot Model

When the pilot is confronted with a two-axis tracking task, he will use the same control policy in both channels (Ref 10). Thus, a single pilot model must be developed to replace the lateral pilot model, Eq (57), and the longitudinal pilot model, Eq (100), with $K_p = .8$. The same adjustment rules are used to determine the parameters of this homogeneous pilot model; additionally, the model is constrained to cause the system crossover frequency to occur along a -20 decibel/decade slope in both axes.

The bandwidth of v_g predominates, hence the lateral effective time delay will be used in the homogeneous model. The lag at one second in the longitudinal pilot model will not be included in the homogeneous model because it greatly increases lateral tracking error. Further, close investigation of the longitudinal case reveals that the system goes unstable at $K_p = 1.1$ with the single axis pilot model. Thus, the pilot is unable to take advantage of the extended -20 decibel/decade slope. Removing the lag would cause the pilot to operate in a somewhat more confined -20 decibel/decade region; a benefit, however, is that longitudinal tracking error is reduced when the lag is omitted. Finally, in order to operate

in the middle of a -20 decibel/decade region in the longitudinal case, a pilot gain of $K_p = .6$ must be used; at this gain, the lateral system is also operating on the desired slope.

The above constraints yield the following homogeneous pilot model

$$Y_p = \frac{-.6(s - 16.667)}{(s + 16.667)} \tag{109}$$

Returning to the preceding section on longitudinal tracking, Eq (100) is replaced by Eq (109) and the computations of that section are repeated with the fixed gain homogeneous pilot model. The root mean square values of the longitudinal controlled variables, with pilot remnant included, are determined to be

$$\sigma_\theta = .1308° \tag{110}$$

$$\sigma_{\Delta\alpha} = .1443° \tag{111}$$

In addition to the homogeneous pilot model, another important effect must be considered in the two-axis tracking task. The larger lateral tracking errors interfere with the pilot's ability to sense error and error rate in the longitudinal axis; consequently, longitudinal tracking performance is degraded from that predicted by single axis analysis even with homogeneous pilot models and remnant included. This degradation is called the visual-motor interference and can be expressed analytically as (Ref 16:131-132)

$$\sigma_{\theta_T} = \sqrt{[\sigma_\theta^2 + K_{\theta_\mu}^2 \sigma_\mu^2]} \tag{112}$$

where

σ_{θ_T} = two axis longitudinal tracking error intensity,

σ_μ = single axis lateral tracking error intensity,

K_{θ_μ} = interference coefficient = .558.

Applying this relationship to Eq (110) and Eq (111) yields

$$\sigma_\theta = .2615° \tag{113}$$

$$\sigma_{\Delta\alpha_T} = .2686° \tag{114}$$

Similarly, substituting Eq (109) instead of Eq (57) into Eq (56) and recomputing the root mean square values of the lateral controlled variables and the lateral tracking error yields

$$\sigma_\psi = .4148° \tag{115}$$

$$\sigma_\phi = .6824° \tag{116}$$

$$\sigma_\beta = .5007° \tag{117}$$

$$\sigma_\mu = .4059° \tag{118}$$

Investigation of the forward transfer functions reveals that the operating frequencies are .72 radians/second in the longitudinal case and .0012 radians/second in the lateral case.

The six equations listed above are the completed longitudinal and lateral tracking error models, respectively, for the example firing situation. Thus, for a given level of gust inputs, the tracking error in both axes has been predicted. The final task, to be accomplished in the next chapter, is to quantitively evaluate the terminal miss distance caused by these tracking errors.

Special Longitudinal Case

Occasionally, the pilot is forced to track and fire with a fixed sight instead of the lead-computing sight. In this situation, the sight display indicates a correct firing solution for only one case as the pipper remains depressed at a constant angle regardless of the state of either the target aircraft or the attacking aircraft. For the purposes of this study, it will be assumed that the fixed depressed reticle is indicating the correct

aim point in the example firing situation; the object of this investigation is to remove the dynamics of the fire control system and to determine the effect that this action will have on the longitudinal and lateral tracking performance.

The analysis proceeds by removing the fire control components from the system illustrated in Fig. 15 and, consequently, omitting the terms of Eq (97) from the appropriate entries of Eq (90). Paralleling the procedure contained in the Longitudinal Tracking section, calculations reveal that the pilot observes a disturbance input with a bandwidth of 1.0 radians/second and the plant has a -20 decibel/decade slope from a frequency of 0.0 radians/second to a frequency of .98 radians/second.

This information, coupled with the information derived in the Lateral Tracking section, dictates the following homogeneous pilot model:

$$Y_p = \frac{-.1(s-16.66)}{(s+16.66)} \tag{119}$$

Repeating the computations outlined in the preceding section with the pilot model given by Eq (119), the following root mean square values are predicted for longitudinal and lateral tracking error:

$$\sigma_\theta = .2656° \tag{120}$$

$$\sigma_\mu = .4057° \tag{121}$$

Bode plots of the forward transfer functions reveal that both closed loop systems are operating on -20 decibel/decade slopes at frequencies of .08 radians/second in the longitudinal case and .0004 radians/second in the lateral case.

IV. Mathematical Model of the Aerial Gunnery Task

Introduction

In this chapter the prediction angle will be defined and the parameters of the nominal lead-pursuit trajectory will be calculated for the example firing situation. Then, the attacking aircraft will be disturbed from its nominal state by gust inputs. The cannon will be fired from this perturbed state and the projectile terminal miss distance resulting from the errors in the tracking and controlled variables of the perturbed state will be determined.

Prediction Angle

Description. In order to hit a moving target with an aircraft-mounted cannon, it is necessary to create the proper angle between the tracking line and the weapon line. This angle is called the prediction angle and consists of the following components (Ref 22:2)

- lead
- curvature correction
- jump correction

Lead. For the projectile to strike the target, the component of the projectile velocity perpendicular to the tracking line must be equal to the component of the target velocity perpendicular to this same line. Figure 17 presents the two dimensional case.

From Fig. 17,

$$\vec{V}_p \sin L = \vec{V}_T \sin \rho \tag{122}$$

Hence,

$$L = \arcsin \left\{ \frac{\vec{V}_T \sin \rho}{\vec{V}_p} \right\} \tag{123}$$

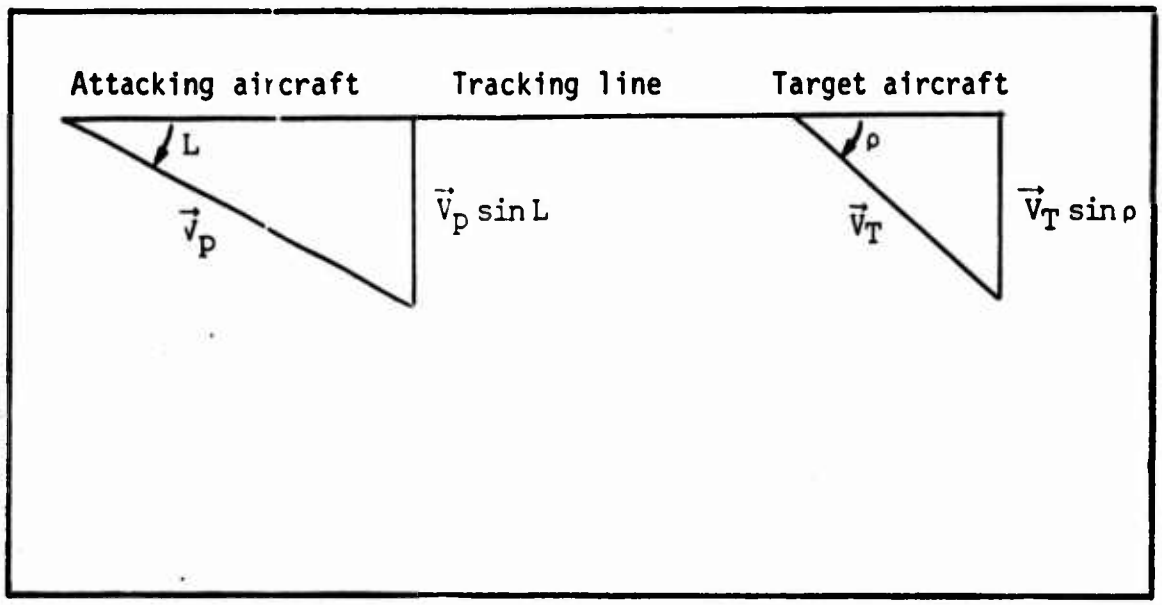

Fig. 17. Lead Angle Geometry

where

L = lead angle,

$\vec{V}_p$ = projectile total velocity

ρ = target angle off, and

$\vec{V}_T$ = target velocity (Ref 2:3)

Curvature Correction. There are three components of curvature correction:

The wind curvature angle is zero in the aerial gunnery situation as the attacking aircraft, the target aircraft, and the projectile are all moving in the same air mass. In firing at a ground target, however, a left crosswind would cause the ground track of the projectile to move to the right as it travels to the target. In the example firing situation, wind curvature is ignored.

The drift correction angle is caused by the interaction of the torque produced by the aerodynamic lift acting on the projectile and the angular momentum of the projectile due to spin. The result of this action is a

"drift" of the projectile to the right if the spin is to the right. The effect of this interaction is small and can be neglected (Ref 2:6).

The gravity drop angle is the result of the action of gravitational acceleration upon the projectile during its time of flight. The situation is depicted in Fig. 18 (Ref 2:7).

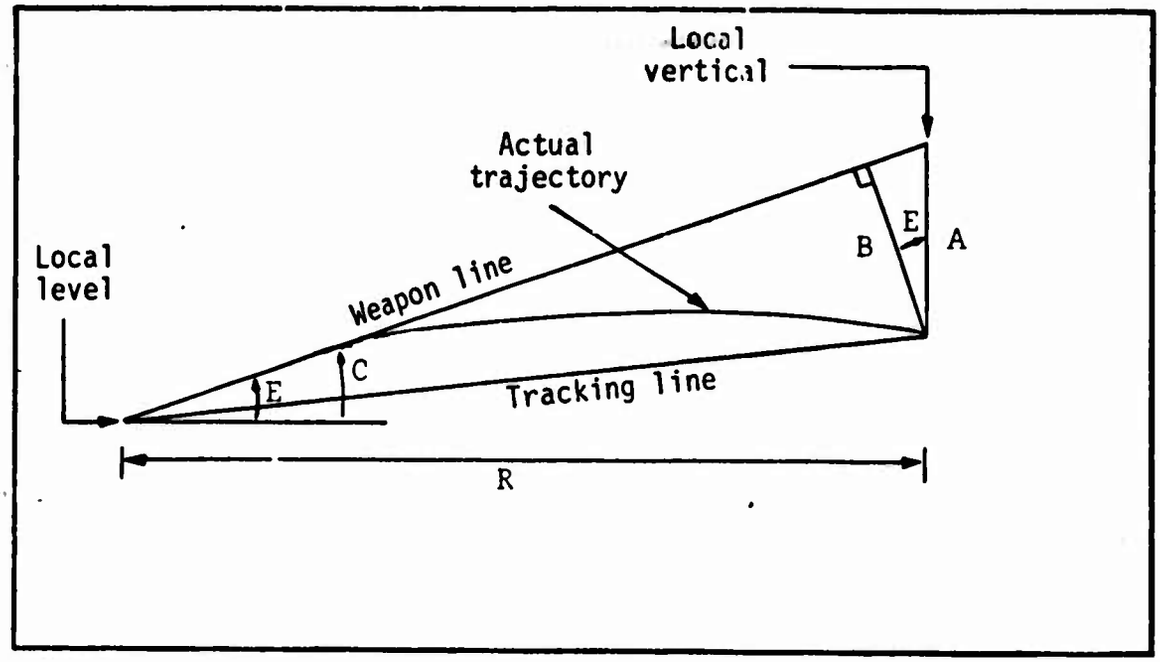

Fig. 18. Gravity Drop Geometry

From Fig. 18,

$$A = \frac{1}{2} g t_f^2 \tag{124}$$

$$B = \frac{1}{2} g t_f^2 \cos E \tag{125}$$

Hence,

$$\sin C = \frac{\frac{1}{2} g t_f^2 \cos E}{R} \tag{126}$$

and

$$t_f = \frac{R}{V_{PA}} \tag{127}$$

Thus,

$$C = \text{arc sin} \left\{ \frac{gR \cos E}{2V_{PA}^2} \right\} \tag{128}$$

where

t_f = projectile time of flight,

g = gravitational acceleration constant,

Σ = elevation angle of weapon line above the local horizontal,

R = target range,

C = gravity drop angle, and

V_{PA} = average projectile velocity.

Jump Correction. There are two components of the jump correction angle:

The windage jump angle is created by the misalignment of the weapon line and the aircraft velocity vector. As the projectile leaves the muzzle and enters the airstream, it has an angle of attack and experiences a net lift force. This lift force inclines the true projectile path away from the weapon line towards the aircraft velocity vector. This term can be neglected in the aerial gunnery situation (Ref 2:3).

The velocity jump angle is a consequence of the fact that the total projectile velocity is the vector sum of the muzzle velocity vector and the aircraft velocity vector. Figure 19 is a geometric description of velocity jump (Ref 2:4).

From Fig. 19,

$$\sin J = \frac{X}{V_p} = \frac{\sin \xi \, V}{V_p} \tag{129}$$

$$J = \text{arc sin } \frac{\sin \xi \, V}{V_p} \tag{130}$$

where

J = jump angle,

ξ = angle between the muzzle velocity vector and the aircraft velocity vector,

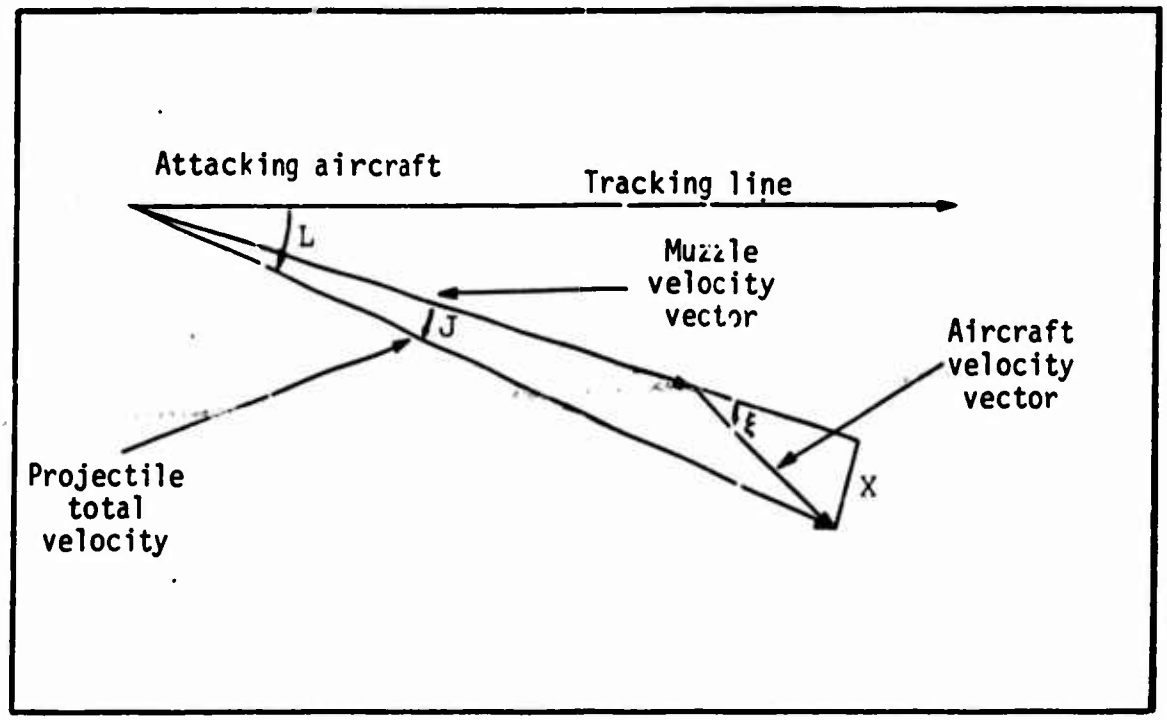

Fig. 19. Velocity Jump Geometry

V = aircraft velocity vector, and

V_p = projectile total velocity.

Determination of the Nominal Trajectory

Introduction. The parameters of the nominal lead-pursuit trajectory are determined by an iterative algorithm on the digital computer. This method of solution is dictated by the fact that no closed-form solution of the prediction angle equation exists when projectile drag and aircraft angle of attack perturbations are included in the mathematical model, and these latter effects must be considered if the example firing state is to be a realistic situation.

The calculation of the firing state parameters will be described briefly in this section. The intent is to follow the mathematical flow of the digital computer program explaining in detail unusual or interesting aspects of the computations. Finally, the parameters of the nominal lead-pursuit trajectory will be stated.

Calculation of Prediction Angle. The calculations are initiated by establishing a tracking line from the attacking aircraft to the target aircraft. Then the target aircraft's velocity vector is resolved into the tracking line reference system described in Chapter II. Once the velocity components of the target aircraft are known in the tracking line reference system, Eq (123) is applied in the TLY and TLZ axes to determine azimuth and elevation lead angles, respectively.

Then, the angle of attack necessary to maintain level, unaccelerated flight in the example firing situation is substituted into Eq (130) to determine the jump correction in the elevation plane.

There are two noteworthy aspects of the jump correction angle.

First, the angle ξ must be defined and measured with care. As illustrated in Fig. 20, two distinct situations can occur.

In the first case, the weapon line is between the tracking line and

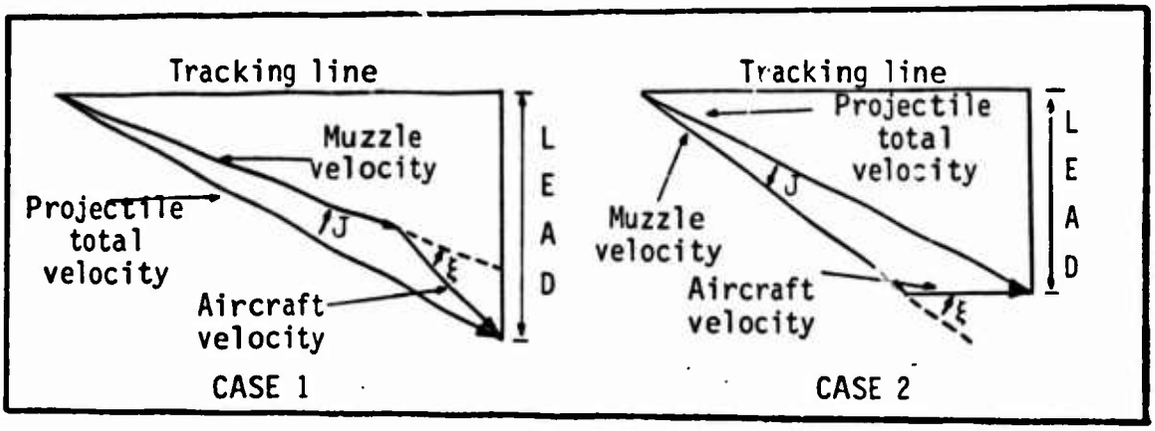

Fig. 20. Jump Angle Condition

the aircraft velocity vector and the jump angle is subtracted from the total lead angle; in the second case, the weapon line does not lie between the tracking line and the aircraft velocity vector and the jump angle is added to the total lead angle. Consequently, when the cannon muzzle is depressed below the aircraft velocity vector, ξ will be considered negative

and when the weapon line is elevated above the aircraft velocity vector, ξ will be considered to be positive.

Second, it is assumed that, in the nominal firing situation, the tracking line, the weapon line, and the attacking aircraft's velocity vector all lie in the elevation plane of the attacking aircraft; thus, the jump angle correction occurs in the aircraft longitudinal plane. Now, since the total lead angle is created and maintained by pitch control, the jump correction angle is either added to or subtracted from the total lead angle. It should be noted, however, that the attacking aircraft's velocity vector can be displaced out of the longitudinal plane by introducing sideslip. The F-4 fire control system cannot compensate for this condition. Thus, this situation is an error producing state and will be considered to be a perturbation from the nominal firing position.

Finally, the gravity drop is calculated using Eq (128). Note that in the first iteration, the projectile initial velocity rather than the projectile average velocity is used in Eq (128).

The vector addition of these three angles forms the prediction angle; however, this first prediction angle must be corrected for projectile drag and aircraft angle of attack.

Correcting the Prediction Angle for Projectile Drag. Aerodynamic drag acts to continuously reduce the velocity of the projectile during its time-of-flight. This velocity reduction in turn, alters the lead angle and the gravity drop terms. Therefore, it is necessary to determine the projectile average velocity and time of flight in order to calculate the correct prediction angle.

The drag force on the projectile is (Ref 17:149-150)

$$D = \frac{C_D \rho V^2 S}{2} \tag{131}$$

where

C_D = coefficient of drag,

S = suitable scaling area,

ρ = atmospheric density, and

V = projectile speed.

From Mechanics,

$$F = ma \tag{132}$$

$$ma = -\frac{C_D \rho V^2 S}{2} \tag{133}$$

$$a = -\frac{C_D \rho V^2 S}{2m} \tag{134}$$

where

m = projectile mass, and

a = projectile acceleration.

$$a = -\frac{K\rho V^2}{2} \tag{135}$$

where

$$K = \frac{C_D S}{m} \tag{136}$$

a = deceleration of projectile.

Now,

$$a = \frac{dV}{dt} = -\frac{K\rho V^2}{2} \tag{137}$$

Separating variables,

$$\frac{dV}{V^2} = -\frac{K\rho}{2}\, dt \tag{138}$$

Integrating,

$$-\frac{1}{V} = -\frac{K\rho t}{2} - \frac{1}{V_0} \tag{139}$$

Hence,

$$V = \frac{2V_0}{(2 + K\rho V_0 t)} \tag{140}$$

Also,

$$V = \frac{dR}{dt} = \frac{2V_0}{2 + K\rho V_0 t} \tag{141}$$

$$dR = \left(\frac{2V_0}{2 + K\rho V_0 t}\right) dt \tag{142}$$

Integrating,

$$R = \frac{2}{K\rho} \ln\left(1 + \frac{K\rho V_0 t}{2}\right) \tag{143}$$

Rearranging,

$$R = \frac{2}{K\rho} \ln\left(\frac{V_0}{V}\right) \tag{144}$$

and

$$t = \frac{2e^{(K\rho R/2)} - 2}{K\rho V_0} \tag{145}$$

and

$$V = V_0 e^{-(K\rho R/2)} \tag{146}$$

At this point, K must be determined. Rearranging Eq (144) and substituting for the following variables (Ref 14:49):

$$K = \left(\frac{2}{R\rho}\right) \ln\left(\frac{V_0}{V}\right) = .2011083 \text{ ft}^2/\text{slug} \tag{147}$$

where

V_0 = 4000 ft/sec,

V = 2000 ft/sec at R = 2900 ft, and

ρ = .002377 slug/ft at sea level.

To correct the prediction angle for projectile drag, the bullet time-of-flight is determined from Eq (145) and the final velocity from Eq (146).

An average velocity is then determined and an augmented range is formed by adding the target distance covered during the projectile's time-of-flight to the original distance. This iterative procedure is continued until two successive augmented ranges meet some stopping criterion. The average velocity is then used to create another lead angle and the new time-of-flight and average velocity are used to compute gravity drop. Now, since the increased lead angle has reduced the bullet's forward velocity, another iterative loop is activated which corrects the prediction angle for drag again. This outer loop runs until two successive times-of-flight are within some stopping criterion. At this point, the prediction angle is corrected for projectile drag.

Correcting the Prediction Angle for Angle of Attack. The aircraft angle of attack affects ξ, the angle between the weapon line and the attacking aircraft's velocity vector. Consequently, the jump angle and the total lead angle must be corrected for angle of attack.

Angle of attack can be calculated from the attacking aircraft's state. First, an aircraft weight is selected; then the lift required to maintain equilibrium is determined:

$$W = \frac{L \cos \Phi}{\cos \Theta} \tag{148}$$

where

$$L = \frac{C_{L_T} \rho V^2 S}{2} \tag{149}$$

The previously generated prediction angle yields the aircraft bank angle, Φ, and pitch attitude, Θ. The aircraft speed is specified, density is determined from the specified altitude, and S is known for the F-4E. This allows us to solve Eq (148) for C_{L_T},

$$C_{L_T} = \frac{2W \cos \Theta}{\cos \Phi \, SV^2 \rho} \tag{150}$$

For the particular attacking aircraft state, curves of C_{L_T} vs α will yield the angle of attack. Since the cannon is depressed 3 degrees below the wing zero lift line (Ref 11),

$$\xi = \alpha - 3^\circ \tag{151}$$

The value of ξ is used to generate a corrected prediction angle; this new prediction angle yields a different angle of attack. Consequently, an iterative procedure, using the closeness of two succeeding values of ξ as a stopping criterion, is used to correct the prediction angle for attacking aircraft angle of attack.

The method used to determine the coefficient of lift (C_L) implies that available aircraft thrust is sufficient to offset all lift loss due to pitch attitude. This is true only for a limited range of pitch attitude, G-load, airspeed states. Exceeding this envelope will result in aircraft deceleration.

Further, the attacking aircraft and the target aircraft are considered to be in equilibrium. This state is valid only in a small number of aerial gunnery situations. Nevertheless, situations do occur where the attacking aircraft has excess thrust and the target is in unaccelerated flight and, hence, this situation is a valid example firing situation.

Computed Example Firing Situation. Once the prediction angle is corrected for projectile drag and aircraft angle of attack, the parameters of the static firing situation can be determined. The aircraft geometry, angle of attack, and the prediction angle can be used to determine the aircraft pitch attitude in stability axes. The roll angle control requirement dictates the bank angle. The prediction angle iterative solution generates an entire set of projectile solution data. Table II lists the parameters of the nominal firing situation.

TABLE II

Example Firing Situation Parameters

Attacking aircraft:	
Wing angle of attack	1.52 deg
G-load	1.00
Sight depression angle	9.91 mils
Sight deflection angle	0.00 mils
Attitude (stability axes):	
Heading (yaw)	0 deg
Pitch	2.01 deg
Roll	0 deg
Projectile:	
Muzzle velocity	3380 ft/sec
Initial velocity	4331.38 ft/sec
Initial range	2000 ft
Final velocity	2915.97 ft/sec
Final range	2630.12 ft
Average velocity	3530.82 ft/sec
Time of flight	.7449 sec

Calculation of Projectile Miss Distance

If the aircraft cannon is fired when the attacking aircraft is perturbed from the nominal lead-pursuit trajectory, the projectiles will miss the target. The determination of terminal miss distance is rather straightforward and proceeds in the following manner.

First, the aircraft is placed on the nominal trajectory in the computer algorithm and then it is perturbed from this state. The disturbed state is generated by combining the nominal aircraft controlled variables with the variances of the perturbation controlled variables determined in Chapter III (Eqs 113-118); however, great care must be exercised to maintain

the proper interaction of the perturbation controlled-variable variances. The correct perturbed state is created by combining the longitudinal variances as shown in Fig. 21 and the lateral variances as shown in Fig. 22.

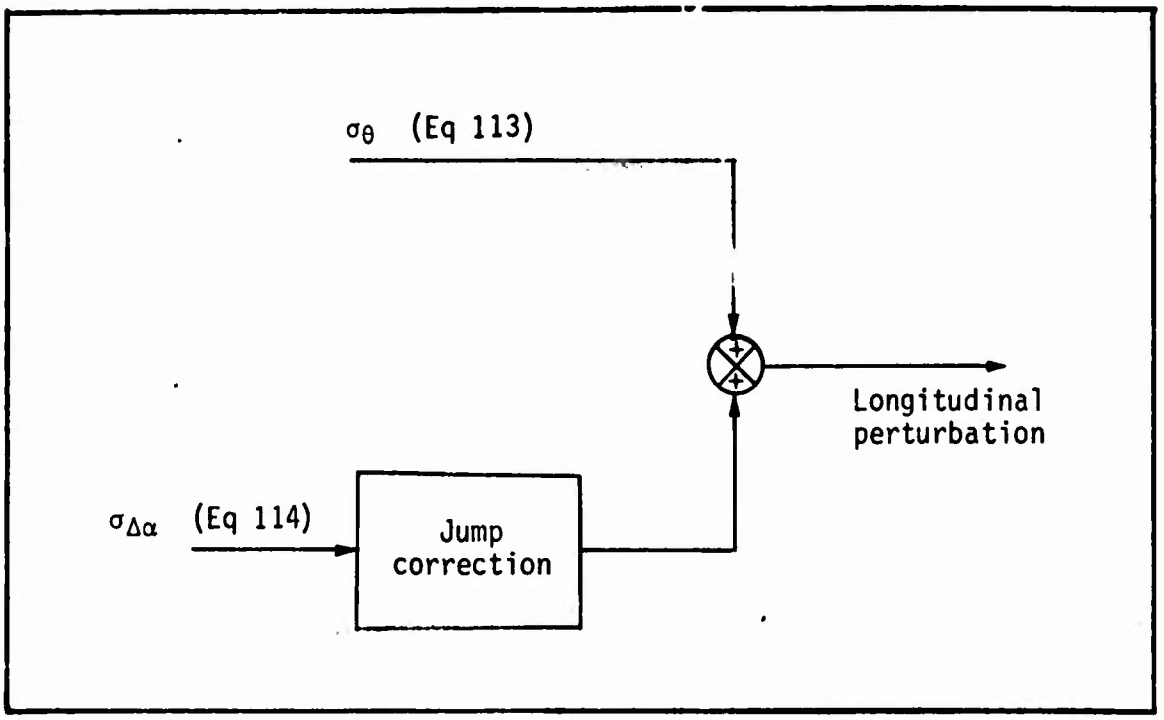

Fig. 21. Longitudinal Variance Interaction

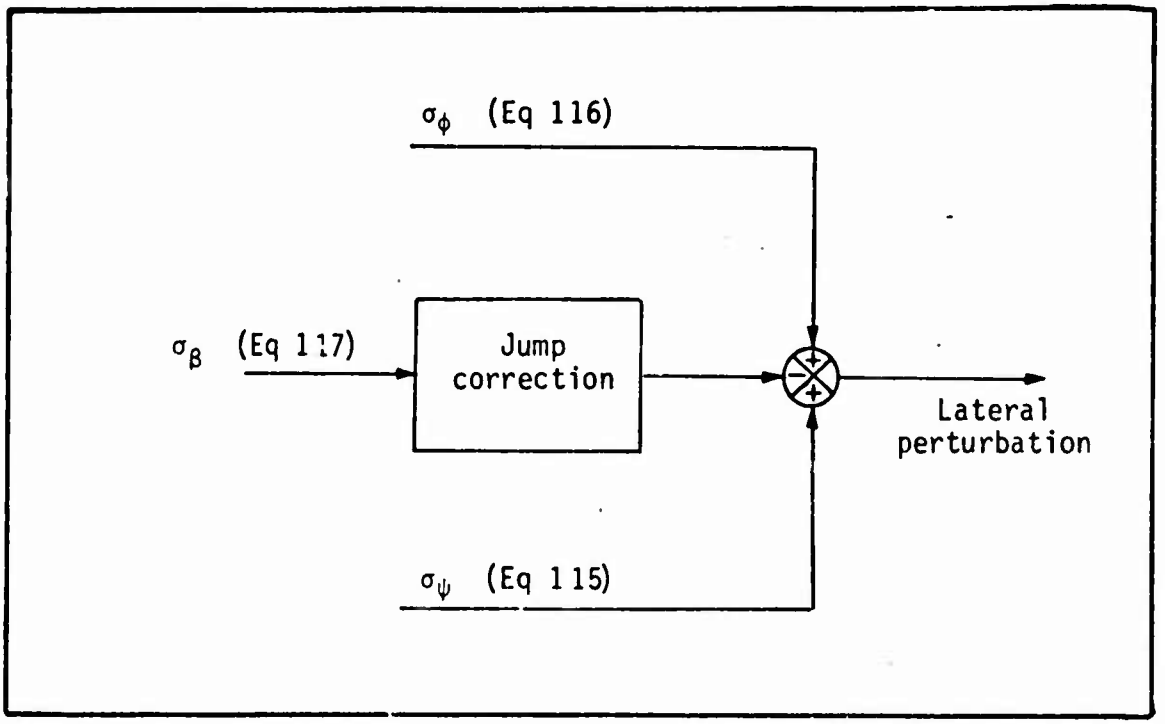

Fig. 22. Lateral Variance Interaction

Then, the projectile is fired from this perturbed state and gravitational acceleration and aerodynamic drag force act on it during the time of flight. The target terminal position is determined and the closest approach of the projectile is calculated. Finally, the total miss distance is resolved into elevation and azimuth miss.

For the example firing situation, the miss distance computation yields

$$\text{elevation miss} = 8.62 \text{ ft} \tag{152}$$

$$\text{azimuth miss} = 23.56 \text{ ft} \tag{153}$$

Equations (152) and (153) represent the completion of the analytical portion of this study. The entire process consists of disturbing the attacking aircraft from its nominal lead-pursuit trajectory, determining the size of the perturbations in the controlled variables with the pilot actively attempting to zero these errors, and finally, propagating these tracking errors into terminal miss distance. The significance and sources of the projectile miss distance will be discussed in the next chapter.

This method of determining miss distance is not rigorous and, in effect, uses a statistical characteristic of random variables, the variances of the controlled variables, as deterministic quantities. There is no guarantee that the correct phasing or proper magnitudes of the perturbed variables are accurately represented by this procedure. It does, however, give a qualitative feel for terminal miss distance, and one can use this data to decide whether terminal error is significant enough to warrant the expenditure of time and money to correct system deficiencies. Moreover, the controlled-variable and tracking variable intensities do provide an accurate measure of system performance and can be used to evaluate system improvements.

To correctly determine terminal miss distance would require a rather complex simulation of the example firing situation and this task could not be accomplished within the limits of this study.

V. Conclusions and Recommendations

Introduction

In this chapter, the results of the analysis will be evaluated and then compared with the baseline case of strafing in an F-4C (Ref 17: 143-146). Next, recommendations for extensions of this study will be given; finally, some general remarks on certain mechanical aspects of the analysis theory will be made.

Analysis of Results

The objective of this study was to develop a model of the pilot-aircraft system which related the pilot tracking performance to the aircraft dynamics. This was accomplished by developing two mathematical models which demonstrated the propagation of a disturbance input through the pilot-aircraft system to the aircraft controlled variables.

In the longitudinal case, the analysis showed that perturbation pitch attitude, the longitudinal tracking variable, had a root mean square intensity of 0.1308° and the perturbation angle of attack had an rms intensity of 0.1443°. If remnant threshold is defined to be the rms intensity of pilot controlled output in the absence of a disturbance input, Eq (74) can be used to calculate a threshold value of .1118°. It then becomes evident that remnant accounts for approximately 90% of the longitudinal tracking error; therefore, it is of questionable value to alter the longitudinal dynamics to achieve only small increases in tracking accuracy.

In the lateral case, however, Eqs (115) through (118) demonstrate that remnant accounts for only 20% to 33% of the rms intensity of the controlled variables and, thus, the improvement of lateral dynamics would

significantly reduce pilot tracking error in the lateral axis. The next question that arises is the determination of the proper method to improve lateral dynamics.

The most obvious method of correcting the deficiencies of the lateral dynamics is to perform a parameter optimization study on the lateral augmentation systems to determine the system gains which will minimize lateral tracking error. A more sophisticated approach would be to investigate different stability augmentation configurations to determine the feedback scheme or blend of schemes which affect the greatest reduction in lateral tracking error.

In Chapter III it was determined that the longitudinal dynamics constrained the homogeneous pilot to operate in a limited range of gains; this resulted from the effects of the dynamics of the fire control system. To illustrate this point, the fire control system dynamics were neglected and a special longitudinal case was analyzed. The results of this section indicate that the lateral pilot model parameters dominate the homogeneous pilot model when the fire control system is disengaged. However, comparison of Eq (115) through (118) with Eq (79) through (82) shows that only a 5% improvement in lateral controlled variable intensities is achieved in this case; additionally, Eq (120) indicates that the rms intensity of the longitudinal tracking error actually increases slightly in this situation. Thus, improvement of longitudinal dynamics will not materially improve lateral tracking error.

In summary, the F-4E lateral dynamics introduce significant lateral tracking errors in the example firing situation and should be augmented to improve mission performance. Conversely, longitudinal tracking error is predominated by pilot remnant and, thus, improvements in aircraft

dynamics will not significantly improve longitudinal tracking performance.

Baseline Comparison

Comparison of the tracking errors in the aerial gunnery situation with those of the baseline strafing mission will give an indication of the capability of the control system to perform different missions and will illustrate control system characteristics which are common to the two missions. The longitudinal tracking error, the perturbation pitch attitude, is larger at .26° in the aerial gunnery case than in the strafing case where it is .17° (Ref 16:133). It should be noted, however, that pilot threshold remnant and visual-motor coupling from the lateral tracking task dominate these longitudinal tracking error values; consequently, longitudinal tracking performance cannot be significantly improved by altering the pitch tracking dynamics.

Similarly, the lateral tracking error is .41° and .16° for the aerial gunnery and strafing tasks, respectively (Ref 16:133). In this case, the lateral tracking error in aerial gunnery is more than double that in strafing and is due primarily to the differences in pilot control policy.

Although the tracking errors are larger in both instances for the aerial gunnery task, the same dynamic characteristic manifests itself in both missions: lateral tracking error predominates. Hence, if lateral tracking error is reduced by altering the lateral tracking dynamics, longitudinal tracking error will also be reduced as a result of the cross coupling effects. A design goal common to both missions, then, is the improvement of lateral tracking dynamics.

Recommendations for Further Study

The purpose of this study was to demonstrate the effect of aircraft dynamics upon pilot tracking capability. As evidenced by the discussion in Chapter II, however, it appears that computational errors in the fire control system may contribute significantly to terminal miss distance. The next step in the analysis of the aerial gunnery mission then would be to model the fire control system and demonstrate its effect on terminal miss distance. The analyst could then focus his attention on the system--flight control or fire control--which had the greater effect upon mission success.

With both systems completely modeled, the sight smoothing could be varied to determine the effect upon longitudinal tracking capability; also, as discussed previously, various augmentation schemes could be employed to reduce lateral tracking error.

Discussion of the Analysis Procedure

The key element in this analysis is the analytical model of the human pilot. The example firing situation was specifically chosen to meet all constraints imposed by this technique. Nevertheless, in several instances during this study, the pilot modeling theory seemed inadequate. In both lateral and longitudinal axes, system dynamics were encountered which were much more complex than the plant dynamics used in the pilot modeling studies. Further, in the longitudinal axes, the pilot was constrained to operate in a narrow frequency range; no data existed to indicate whether the pilot could really operate in such a situation. Finally, all operating frequencies were much lower than those in the studies by McRuer (Ref 12).

Because the analysis theory used in this study has so many potential

applications and because the pilot modeling techniques are such a key element in the theory, it is recommended that further studies using more complex dynamics and requiring operations at lower frequencies be conducted to expand the existing body of knowledge of analytical pilot modeling theory.

Bibliography

1. Blakelock, John H. Automatic Control of Aircraft and Missiles. New York: John Wiley and Sons, 1965.

2. -------. "Fire Control Principles." Unpublished lecture notes. Wright-Patterson Air Force Base, Ohio: Air Force Institute of Technology.

3. Bridges, B. C. and F. M. Krachmalnick. Calculated Lateral-Directional Stability and Performance Characteristics of the F-4B/C/D/J and RF-4B/C Aircraft Plus the AN/ASA-32H Automatic Flight Control System. F935. Saint Louis, Missouri: McDonnell Aircraft Company, September 1968.

4. Chalk, C. R., et al. Background Information and User Guide for MIL-F-8785 (ASG), 'Military Specification - Flying Qualities of Piloted Airplanes.' AFFDL-TR-69-72. Wright-Patterson Air Force Base, Ohio:

5. Eshback, O. W. Handbook of Engineering Fundamentals. New York: John Wiley and Sons, May 1963.

6. Etkin, Bernard. Dynamics of Flight. New York: John Wiley and Sons, May, 1967.

7. General Electric Company. Air-to-Air Gunnery Improvement for the F-4E Per FSCP-34. ACD 9986. Binghamton, New York: Avionics Controls Department, August, 1970.

8. General Electric Company. Multimode Flight Control Definition Study. ACD 9690. Binghamton, New York: Aircraft Equipment Division, 1970.

9. Levison, W. H. The Effects of Display Gain and Signal Bandwidth on Human Controller Remnant. AMRL-TR-70-93. Wright-Patterson Air Force Base, Ohio: Aerospace Medical Research Laboratory, March 1971.

10. ------ and J. I. Elkind. Studies of Multi-Variable Manual Control Systems: Two Axis Compensatory Systems with Compatible Integrated Display and Control. CR-554. Washington: National Aeronautics and Space Administration, August 1966.

11. Mackacek, E. C., K. Williams, and T. Bronson. Calculated Longitudinal Stability and Performance Characteristics of the F/RF-4E Aircraft Plus the AN/ASA-32J Automatic Flight Control System. E934-Addendum I. Saint Louis, Missouri: McDonnel Aircraft Company, May 1970.

12. McRuer, D. T. and H. R. Jex. "A Review of Quasi-Linear Pilot Models." Transactions on Human Factors in Electronics. Institute of Electrical and Electronics Engineers, Vol 8, 1967.

13. -------. A Systems Analysis Theory of Manual Control Displays. NASA, SP-144. Third Annual NASA-University Conference on Manual Control, 1967.

14. Mehserle, H. J. Capability of the F-4C Aircraft/SUU-16/A Gun Pod in the Close Air Support Role. APGC-TR-65-57. Eglin Air Force Base, Florida: Air Proving Ground Center, August 1965.

15. Quinlivan, R. P. Multimode Flight Control Definition Study for Precision Weapon Delivery. AFFDL-TR-71-39. Wright-Patterson Air Force Base, Ohio: Air Force Flight Dynamics Laboratory, June 1971.

16. Rankine, Robert R., Jr., et al. Analysis of Piloted Weapon Delivery. Paper presented at National Aerospace Electronics Conference, Dayton, Ohio: Air Force Institute of Technology, May 1972.

17. Rankine, Robert R., Jr. "The Effects of Aircraft Dynamics and Pilot Performance on Tactical Weapon Delivery Accuracy." PhD dissertation, University of California, Los Angeles, California, 1970.

18. -------. "Notes on Manual Flight Control." Unpublished lecture notes. Air Force Institute of Technology, Wright-Patterson Air Force Base, Ohio, July 1971.

19. ------- and C. T. Leondes. "Modeling the Effects of Pilot Performance on Weapon Delivery Accuracy." Journal of Aircraft, 9:286-293 (April 1972.

20. T. O. 1F-4E-34-1-1. Aircrew Weapons Delivery Manual (Non-Nuclear). Wright-Patterson Air Force Base, Ohio, June 1968.

21. Truxal, John G., ed. Control Engineer's Handbook. New York: McGraw-Hill, 1958.

22. Wrigley, W. and John Hovorka. Fire Control Principles. New York: McGraw-Hill Book Co., 1959.

23. Wylie, C. R., Jr. Advanced Engineering Mathematics. New York: McGraw-Hill Book Co., 1958.

Appendix A

F-4E Aircraft Characteristics

This appendix serves as a compendium of information of the characteristics of the F-4E aircraft in the example firing situation. The F-4E can be mathematically described by its dimensions, its control system dynamics, and the coefficients of its equations of motion at a particular flight condition. The flight condition of interest in this study is the nominal lead-pursuit trajectory of the aerial gunnery mission; the parameters of this state are

h = 15,000 ft above mean sea level = altitude

M = .9 Mach = Mach number

U_0 = 951.63 ft/sec = velocity

ρ = .001496 slugs/ft^3 = air density (Ref 6:497)

The dimensions of the aircraft at this flight condition are (Refs 3 and 11)

W = 46,159 pounds = aircraft weight

ϵ = 2 degrees = gun depression angle below the fuselage reference line

I_x = 28,203 slugs ft^2 = moment of inertia about the X axis

I_y = 164,258 slugs ft^2 = moment of inertia about the Y axis

Iz = 153,899 slug ft^2 = moment of inertia about the Z axis

I_{xz} = 4427 slug ft^2 = product of inertia

$\bar{c}$ = 16.04 ft = mean aerodynamic chord

s = 530 sq ft = reference wing area

b = 38.41 ft = wing span

The dimensional aerodynamic coefficients for the equations of motion written in stability axes, Eqs (90) and (20), are listed below for the example firing state. The longitudinal axes stability coefficients are (Ref 11:13)

α_{w_T} = 1.8 degrees = trim wing angle of attack

C.G. = 31.9% = center of gravity expressed as a percentage of mean aerodynamic chord

Z_α = - 1.0326

$Z_{\dot{\theta}}$ = -.005291

Z_δ = -.09512

$M_{\dot{\alpha}}$ = -.3439

M_α = -10.443

$M_{\dot{\theta}}$ = -.7381

M_δ = -37.08

The lateral-directional axes stability coefficients are (Ref 3:24)

L_p = - 1.972	Y_p = .0002
L_r = .5334	Y_r = - .9982
L_β = - 21.00	Y_β = - .1886
L_{δ_r} = 4.102	Y_{δ_r} = .0250
L_δ = 13.57	Y_δ = - .0040
N_p = - .0314	Y_ϕ = .0338
N_r = - .4674	N_{δ_r} = - 5.039
N_β = 10.73	N_δ = .3857

It should be noted that the subscript δ indicates the combined effective displacement of spoilers and ailerons for the F-4E; in this study it will be referred to simply as aileron deflection.

The elevon control system of the F-4E is illustrated in Fig. 23 (Ref 17:155).

The control law for this system is

$$\delta_e = -\frac{16\delta_{PE}}{s+20} + \frac{9245s\,\dot{\vartheta}}{(s+1)(s+20)(s+40)(s+76.9)} \qquad \text{(A-1)}$$

This can be expressed as

$$\delta_e = G(s)[K(s)\delta_{PE} + H(s)\dot{\epsilon}(s)] \qquad \text{(A-2)}$$

where

$$G(s) = \frac{20}{s+20} \qquad \text{(A-3)}$$

$$K(s) = -.8 \qquad \text{(A-4)}$$

$$H(s) = \frac{462.5s}{(s+1)(s+40)(s+76.9)} \qquad \text{(A-5)}$$

The rudder control system of the F-4E is depicted in Fig. 24 (Ref: 17:156).

The control law for the system is

$$\delta_r = \frac{13.6\delta_{PR}}{(s+20)} + \left[\frac{2.435s^2 + 259.0s + 108.6}{(s+.5)(s+20)}\right]r + \frac{217.8s\beta}{(s+20)} \qquad \text{(A-6)}$$

This can be expressed as

$$\delta_r(s) = C(s)[\delta_{PR}(s) + D(s)r(s) + E(s)\beta(s)] \qquad \text{(A-7)}$$

where

$$C(s) = \frac{13.6}{s+20} \qquad \text{(A-8)}$$

$$D(s) = \frac{.179s^2 + 19.09s + 8.0}{(s+.5)} \qquad \text{(A-9)}$$

$$E(s) = 16.0s \qquad \text{(A-10)}$$

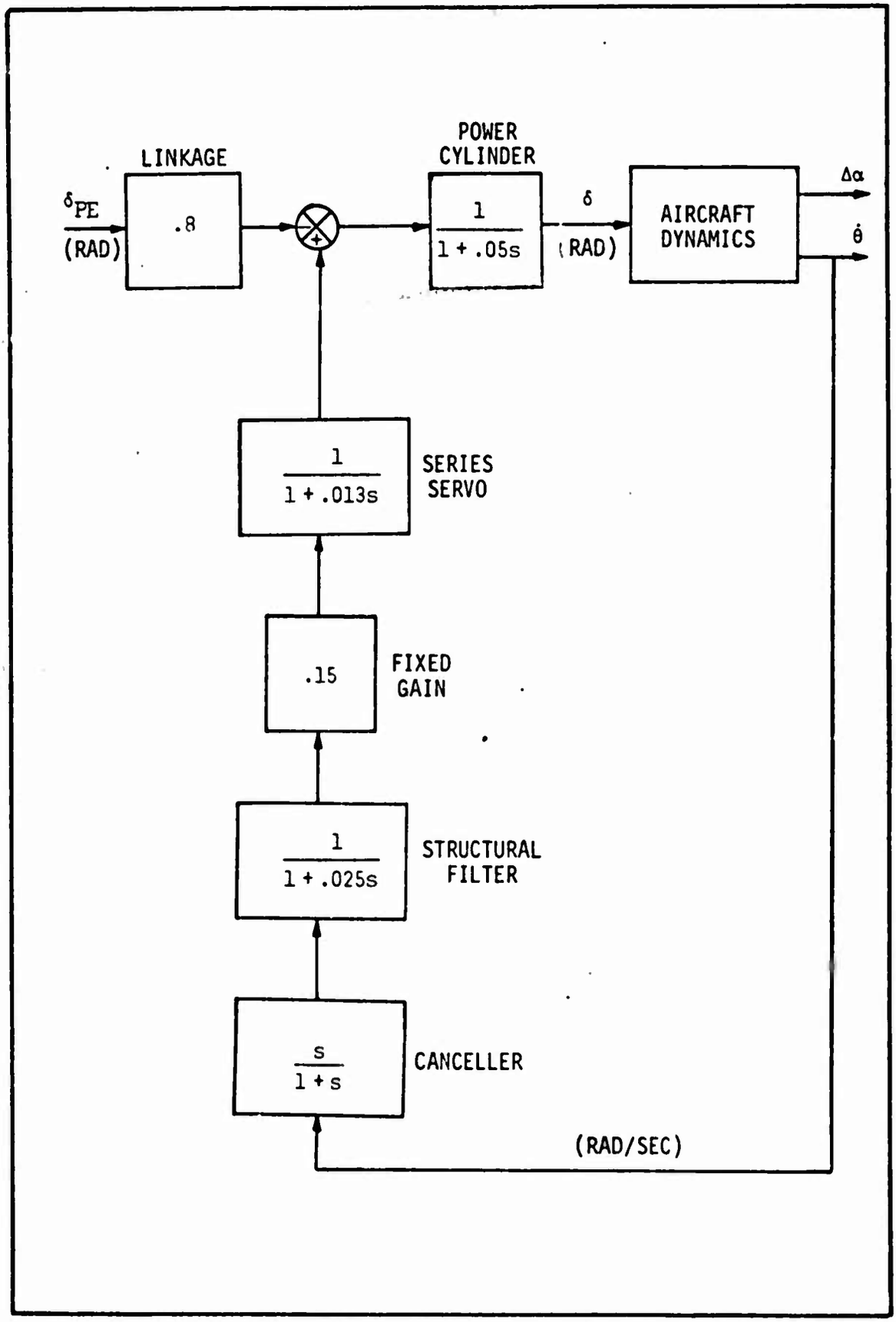

Fig. 23. F-4E Elevon Control System (Adapted from Ref 17:155)

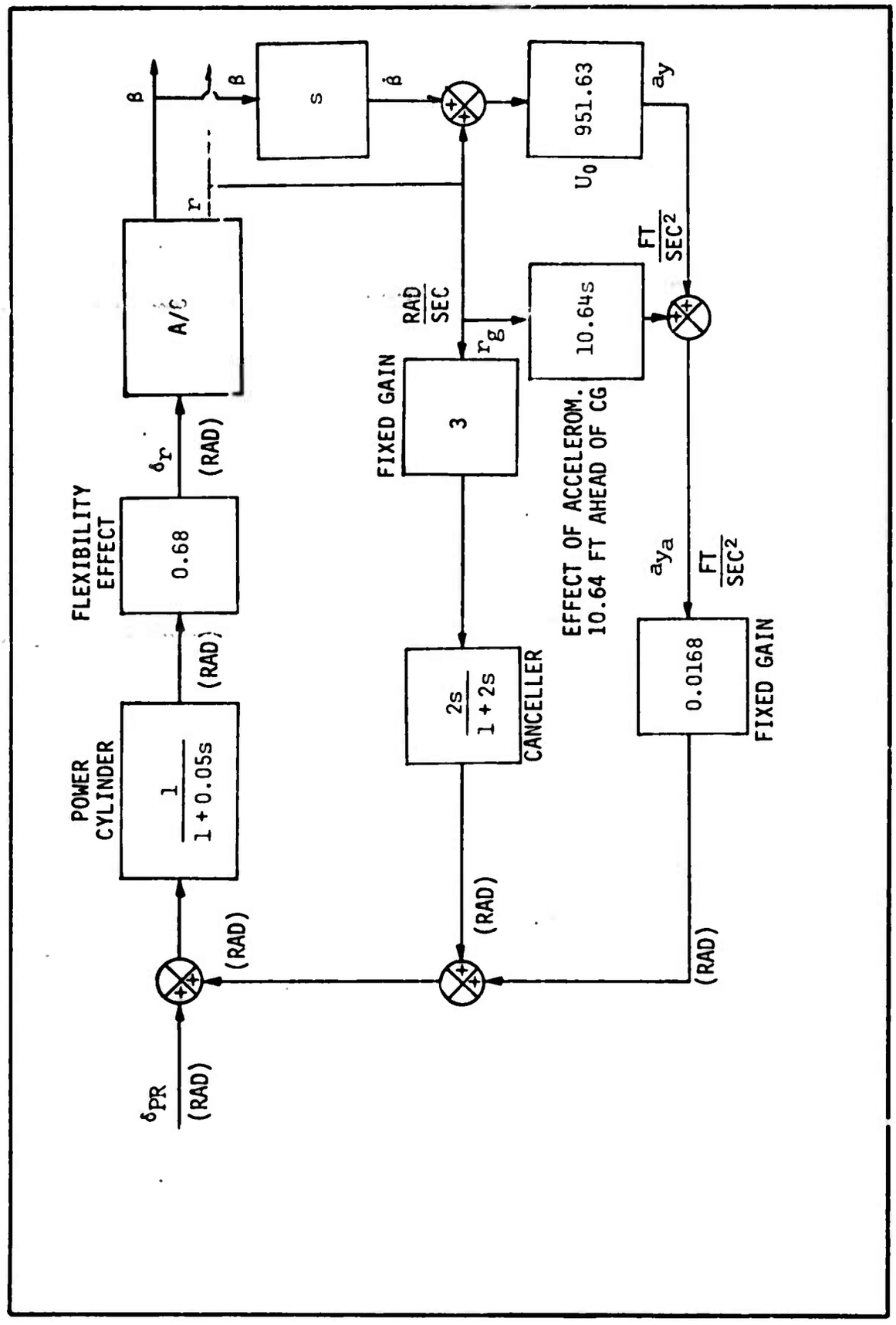

Fig. 24. F-4E Rudder Control System (Adapted from Ref 17:156)

The aileron control system of the F-4E is described in Fig. 25 (Ref 17:157).

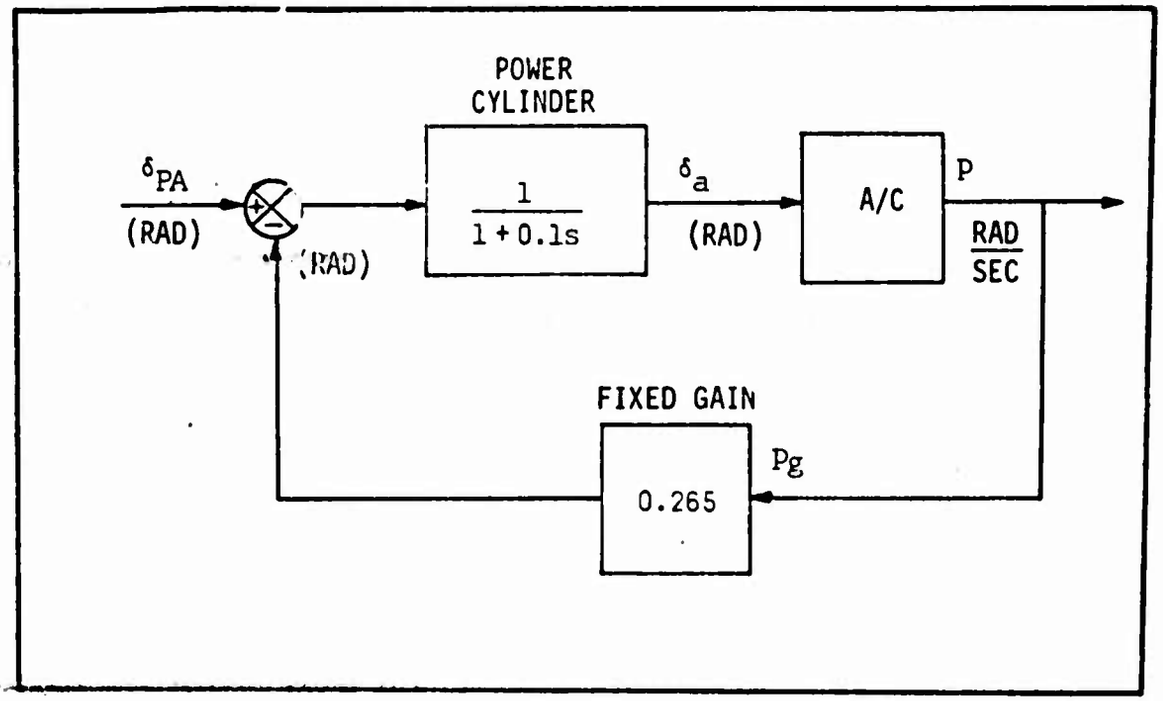

Fig. 25. F-4E Aileron Control System (Adapted from Ref 17:157)

The control law for the system is

$$\delta_a = \frac{10\delta_{PA}}{s+10} - \frac{2.65p}{s+10} \qquad \text{(A-11)}$$

This can be expressed as

$$\delta_a = A(s)[\delta_{PA}(s) - B(s)p] \qquad \text{(A-12)}$$

where

$$A(s) = \frac{10}{s+10} \qquad \text{(A-13)}$$

$$B(s) = .265 \qquad \text{(A-14)}$$

Vita

Richard H. Heckford, Jr [redacted] His father was an Air Force Officer and he moved several times during his childhood. He graduated [redacted] in June 1960 and received a Bachelor of Science Degree, with an Engineering Science Major, upon graduation from the United States Air Force Academy in June 1964. After completing pilot training at Reese Air Force Base, Texas, in August 1965, he attended F-105 gunnery school at Nellis Air Force Base, Nevada. From April until October 1966 he flew 100 missions over North Vietnam with the 469th Tactical Fighter Squadron. Next, he served as a flight training instructor in the T-38 aircraft for two years at Vance Air Force Base, Oklahoma. From 1968 to 1970 he was assigned as a flight test engineer with the Directorate of Guidance Test at Holloman Air Force Base, New Mexico; he entered the Air Force Institute of Technology as a resident student in 1970.

This thesis was typed by Mrs. Virginia Blakelock.